Joint Precoding and On-Board Beamforming for Multiple gateway Multibeam Satellite Systems

Vahid Joroughi, Sina Maleki, Bhavani Shankar M.R., Symeon Chatzinotas, Joel Grotz and Björn Ottersten

***Abstract*— This paper aims to design joint precoding and on-board beamforming of a multiple gateway multibeam satellite system, either in a hybrid space-ground mode, or in a totally on-board one. In such an architecture, with employing high throughput full frequency reuse pattern over both user and feeder links, each gateway serves a cluster of adjacent beams such that the adjacent clusters are served through a set of gateways that are located at different geographical areas. However, such a system brings in two challenges to overcome. First, the interference in both user and feeder links is the bottleneck of the whole system and applying interference mitigation techniques becomes necessary. Second, as the data demand increases, the ground and space segments should employ extensive bandwidth resources in the feeder link accordingly. This entails embedding an extra number of gateways aiming to support a fair balance between the increasing demand and the corresponding required feeder link resources. To solve these problems, this study investigates the impact of employing a joint multiple gateway architecture and on-board beamforming scheme. It is shown that by properly designing the on-board beamforming scheme, the number of gateways can be kept affordable even if the data demand increases. Moreover, Zero Forcing (ZF) precoding techniques are considered to cope with the interference in both user and feeder links which embed in the following premises: (i) each gateway constructs a part of block ZF precoding matrix, (ii) the satellite and gateways perform the precoding scheme, and (iii) a joint design of ZF precoding and on-board beamforming at the payload of the satellite so that no signal processing scheme is conceived at the gateways. The provided simulation results depict the performance gain obtained by our proposed schemes.**

***Index Terms*—Multibeam satellite systems, multipe gateway systems, on-board beamforming, precoding techniques.**

I. Introduction

A. Motivation

Fixed broadband satellite systems are an integral part of the communications technology, aiming to provide ubiquitous broadband services. Built on the Multiuser Multiple-Input Multiple-Output (MU-MIMO) framework, the use of multiple spot beams in modern broadband satellites have been recently considered by employing fractional frequency reuse among beams [1]. Such systems rely on employing a large number of spot beams instead of a single (global) beam in the coverage area to provide higher spectral efficiency [2].

However, one of the major challenges in multibeam architecture is how to deal with interference in the access network. Indeed, adjacent beams create high levels of interference due to the side lobes of the radiation pattern of beams on the Earth surface. Therefore, typically adjacent beams operate on different frequency bands. In this context, N_c is the essential parameter which corresponds to the number of disjoint frequency bands employed on the coverage area ($N_c \geq 1$).

Another promising technique is to use full frequency reuse pattern ($N_c = 1$) by resorting interference mitigation techniques. In this way, interference mitigation techniques as precoding in the forward link and multi-user detection in the return link have been proposed in the past [3]-[4].

Apart from the already mentioned interference limitation, another major challenge of multibeam systems is to deal with the large spectral demands of the Feeder Link (FL), i.e. the bidirectional link between satellite and the Gateway (GW), whose bandwidth requirements increase as it aggregates the traffic of all users. Keeping a full frequency reuse allocation ($N_c = 1$), the required FL resources can be calculated as

$$\mathrm{B}_{\text{feeder-link}} = N\mathrm{B}_{\text{beam}}, \tag{1}$$

where N is the number of on-board feed signals. The notations B_{beam} and $\mathrm{B}_{\text{feeder-link}}$ are the per-beam and the FL required bandwidths, respectively.

Let us consider a total number of K beams with $N > K$. From (1), it is evident that any user/beam available bandwidth enhancement forces the FL resources to be increased accordingly and, eventually the FL might become the communication bottleneck. Note that, in contrast to the single feed per beam architectures, i.e. $N = K$, applying Multiple Feeds per Beam (MFB) at the payload, i.e. $N > K$, can reduce the scan losses for a large continental coverage areas, and are specially suited for contour beams [1]. Recently, some techniques have been proposed in order to reduce the FL spectrum requirements. One solution is moving the FL from the Ka band to the Q/V band so that a larger available bandwidths can be achieved [5]. Unfortunately, the Q/V carrier frequencies suffer the impact of an extremely large fading and more advanced transmitting schemes at the GW are needed.

Another solution is to employ a Beamforming Network (BFN) at the payload aiming at: i) synthesizing the amplitude and phase modulating the excitation of each on-borad feed in the MFB scheme [6], ii) reducing the FL bandwidth requirements [7] by

$$\mathrm{B}_{\text{feeder-link-onboard}} = K\mathrm{B}_{\text{beam}}, \tag{2}$$

where $\mathrm{B}_{\text{feeder-link-onboard}}$ denotes the FL resources that is required after employing the on-board BFN with $\mathrm{B}_{\text{feeder-link-onboard}} < \mathrm{B}_{\text{feeder-link}}$ and $N > K$. However, the FL resources $\mathrm{B}_{\text{feeder-link-onboard}}$ must be increased with the number of beams, i.e. K. Besides, the volume and calibration requirements of any on-board BFN are currently its main drawback.

Another promising option is the use of on-ground multiple GW architecture. This architecture exploits the multiplexing diversity by reusing all the available FL bandwidth across the different Gateways (GWs) [8]-[9]. In this context, the required FL bandwidth becomes

$$\mathrm{B}_{\text{feeder-link-MG}} = \frac{N}{F}\mathrm{B}_{\text{beam}}, \tag{3}$$

where F is the number of GWs, and $\mathrm{B}_{\text{feeder-link-MG}}$ denotes the FL resources which is required at multiple GW architecture. Indeed, the multiple GW architecture reduces the required FL

resources to $\mathrm{B}_{\text{feeder-link-MG}} < \mathrm{B}_{\text{feeder-link-onboard}}$ with $\frac{N}{F} < K$. Nevertheless, the deployment of several GWs increases the cost of the system. Besides, considering (3), by increasing the demand in the coverage area, a specific number of GWs shall be employed aiming to provide a fair balance between the increased demands and their required FL resources.

B. Previous works

In the context of applying interference mitigation techniques and optimizing FL resources in multibeam networks, the following possible configurations have been developed in the past:

1) *Ground Processing* (GP): a single GW employs an interference mitigation technique to cope with the increased level of inter-beam interference. Satellite payload works in the transparent mode. In this way, the FL needs a total bandwidth of $\mathrm{B}_{\text{feeder-link}}$ as in (1), which is very high [10]-[11].

2) *Hybrid Space-Ground Processing* (HSGP): the ground segment consists of a single GW that embeds interference mitigation techniques to manage the inter-beam interference. The payload employs an on-board BFN to assign $\mathrm{B}_{\text{feeder-link-onboard}}$ as in (2). The authors in [12] have presented a heuristic HSGP scheme where the GW uses a Minimum Mean Square Error (MMSE) interference mitigation technique. To manage FL resources, the authors have foreseen the presence of a fixed on-board BFN with respect to the User Link (UL), i.e. the bidirectional link between satellite and users, channel component variations to keep the payload complexity low. More works on HSGP scheme have appeared in [6],[7].

Remark 1: Throughout this paper the variability of the channel components is due to the change of position of the users in consecutive time instants and atmospheric fading. ■

3) *Multiple GW Processing* (MGP): the GWs employ interference mitigation techniques and the FL resources is optimized with the number of GWs, e.g. $\mathrm{B}_{\text{feeder-link-MG}}$ as in (3). Two MGP configurations are possible: i) each GW handles part of the user bandwidth across all served beams. This is referred to multi-carrier mode. ii) Each GW coordinates all the user bandwidth in a set of adjacent beams. This is referred as the cluster mode. Comparing (i) and (ii) conveys the cluster mode supports different clusters through reusing the same user bandwidth resources, leading to high available bandwidth resources and eventually higher spectral efficiency at each GW. The authors in [8], [9] and [13] have developed different MGP networks in the cluster mode. They have jointly proved that developing interference mitigation techniques in MGP networks entails taking into account the following issues. First, each GW serves a set of adjacent beams. It is referred to a *cluster* of beams. Second, since the data traffic is independently generated at each GW, every GW should precode/decode the signal in a decentralized fashion and transmit through their corresponding FL. For this, each GW can only use specific feed elements. Third, designing the precoding/detecting matrix is sensitive to the UL and FL Channel State Information (CSI) qualities at each GW. Thus, a certain inter-GW communication is required. Moreover, a CSI feedback mechanism between GWs and user terminals should be developed which is robust to the feedback and quantization errors. Forth, the precoding/detecting scheme shall cope with inter-beam interference in the UL and inter-FL interference.

C. Contributions

Beyond the aforementioned multibeam architectures in Section I.B, this paper investigates the forward link of a novel MGP scheme in the cluster mode, where a BFN scheme is applied at the payload such that the FL requirements in (3) reduce to

$$\mathrm{B}_{\text{feeder-link-onboard-MG}} = \frac{K}{F}\mathrm{B}_{\text{beam}}, \tag{4}$$

with $\mathrm{B}_{\text{feeder-link-onboard-MG}} < \mathrm{B}_{\text{feeder-link-MG}}$ in (3) and $N > K$. This is referred as joint BFN and MGP (BMGP) multibeam network. In addition, since the channel components of both UL and FL are varied, this paper focuses on the presence of a fixed BFN which is sufficiently robust to the variations in both UL and FL, aiming at preserving the payload complexity affordable.

To manage the interference of both UL and FL in our proposed BMGP architecture, two approaches are considered:

A) The GWs precod the transmitted signals by a Zero Forcing (ZF) precoding technique so that each GW computes a part of the full precoding matrix. Furthermore, we provide later a distributed design of the aforementioned ZF precoding scheme where each of the satellite and ground segments calculate a part of the full precoding matrix. For the sake of preserving low complexity, we develop the ZF precoding scheme while the perfect CSI of both FL and UL is available at the GWs through the satellite. This assumption comes from the fact that a perfect CSI feedback (with no quantization errors) regime and also a noiseless CSI exchange mechanism among GWs is established in the infrastructure of BMGP architecture. Quantazing the perfect CSI at GWs is beyond the scope of this work.

B) Joint precoding and BFN are implemented at the payload. Some benefits can be realized in this context. First, it is not necessary to establish a CSI feedback mechanism between satellite and the GWs. Second, CSI exchange mechanism is not needed among GWs, leading to a low complex transmitting segment infrastructure. Third, in case of failing one GW, the traffic can be easily rerouted to the satellite through other GWs without applying any extra signal processing schemes at the GWs. Note that, in order to maintain a low complexity at the payload, the joint precoding and BFN scheme can be kept fixed and robust to the channel variations in both UL and FL.

To summarize, the contribution of this paper is to develop joint on-board BFN and precoding scheme in BMGP network where:

a) Several ZF precoding techniques are deployed in the framework of (A) and (B). Note that the availability of CSI of both UL and FL channels are based on configurations presumed in (A) and (B).

(b) A fixed on-board BFN scheme is proposed which is robust to any variation of UL and FL channel components. We examine the compatibility of the proposed on-board BFN with the developed ZF schemes in (A) and (B) as well.

The rest of the paper is organized as follows. Section II presents the signal model. Several BMGP architectures are developed in Sections III, IV which are in the framework of BMGP development in (A). Section V presents a novel BMGP

scheme in the context of (B). Section VI provides numerical results. Finally, we derive our conclusion in Section VII.

Notation: Throughout this paper, the following notation are adopted. Boldface uppercase letters denote matrices and boldface lowercase letters refer to column vectors. $(.)^H$, $(.)^T$ and $(.)^+$ denote Hermitian transpose, transpose matrices and diagonal (with positive diagonal elements) matrix. respectively. $\mathbf{I}_N$ builds the $N \times N$ identity matrix. $(\mathbf{A})_{ij}$ represents the (i-th, j-th) element of matrix $\mathbf{A}$ and $(\mathbf{A})_{K\times K}$ denotes a submatrix of $\mathbf{A}$ of size $K \times K$. The notation $diag$ represents a diagonal matrix. If $\mathbf{B}$ is a $N \times N$ matrix, $\mathbf{A} \leq \mathbf{B}$ implies $\mathbf{A} - \mathbf{B} \leq 0$ is negative semidefinite. A matrix $\mathbf{M}$ is definite negative if the real part of $\mathbf{z}^H\mathbf{M}\mathbf{z} \leq 0$ for any non-zero $\mathbf{z}$. Finally, $\mathrm{E}\{.\}$ and $||.||$ refer to the expected value operator and the Frobenius norm operators, respectively.

II. System Model

Herein, the focus is on the forward link of a BMGP multibeam satellite system in cluster mode, where a single geosynchronous (GEO) satellite with multibeam coverage provides fixed broadband services to a large set of users with N feeds and K beams, configured corresponds to the MFB mode with $N > K$, in a frequency multiplexed fashion.

By employing a Time Division Multiplexing (TDM) scheme, at each time instant, a total of K single antenna users, i.e. exactly one user per beam, is simultaneously served by a set of F GWs. In this context, each GW serves a cluster of adjacent beams, and converts the corresponding FL signals into on-board feed signals through on-board BFN at the satellite. Let us assume that the GWs use a full frequency reuse pattern, (i.e. $N_c = 1$), at both UL and FL. Then, the interference among the beams and Feeder Links (FLs) could be a bottleneck. To deal with the impact of inter-FL interference in BMGP architecture, the following approaches are considered:

i) It is desired that the inter-FL interference can be neglected so that each GW is modelled as communicating with the satellite through an interference-free and perfectly calibrated FL. This assumption relies on the fact that the GWs are sufficiently separated on the earth surface and the FL interference is minimum. Besides, the FL noise is negligible with respect to the UL, see [8] for further details. This is referred to Perfect FL BMGP (P-BMGP) multibeam architecture. For the aforementioned P-BMGP configuration, we develop a novel ZF precoding scheme that is embedded at the GWs so that each GW carries out a part of main precoding operation. On-board BFN is assumed to be fixed at the satellite and resilient to the UL channel component variations.

ii) In contrast to P-BMGP, the BMGP architecture in reality suffers from the impact of strong inter-FL interference in addition to the UL interference. Two configurations will be developed in this context:

(a) We present the design of ZF precoding at the GWs, and the on-board BFN at the satellite for the case that the BMGP networks suffer from the impact of both UL and FL interference. It is referred as hybrid Space-Ground with Non perfect FL BMGP (SGN-BMGP) architecture.

(b) A joint on-board precoding and BFN scheme is developed at the payload of BMGP in the presence of FL and UL channels interference. This is referred to Space processing with Non perfect FL BMGP (SN-BMGP) architecture.

A. Signal model in P-BMGP architecture

For P-BMGP architecture, the received signal at the coverage area can be modeled as

$$\mathbf{y} = \mathbf{H}\mathbf{B}\mathbf{x} + \mathbf{n}, \tag{5}$$

where $\mathbf{y}$ is a $K \times 1$ vector containing the symbols received by K users, one per beam, at a given time instant. The $K \times 1$ vector $\mathbf{x}$ denotes the stacked transmitted signals at all the on-board feeds and the vector $\mathbf{n}$ of size $K \times 1$ contains the stacked zero mean unit variance Additive White Gaussian Noise (AWGN) such that $\mathrm{E}\{\mathbf{n}\mathbf{n}^H\} = \mathbf{I}_K$. The BFN weights are included in matrix $\mathbf{B}$.

In the sequel, $\mathbf{H}$ is the overall $K \times N$ UL channel matrix whose element $(\mathbf{H})_{ij}$ represents the gain of the link between the i-th user (in the i-th beam) and the j-th satellite feed. The matrix $\mathbf{H}$ includes the propagation losses and radiation pattern, and as such is decomposed as

$$\mathbf{H} = \mathrm{diag}\left(\frac{1}{\sqrt{A}_1}, ..., \frac{1}{\sqrt{A}_K}\right)\mathbf{W}, \tag{6}$$

where A_k denotes the propagation losses from the satellite to the k-th user. $\mathbf{W}$ is a $K \times N$ matrix which models the feed radiation patterns, the path loss and the received antenna gain. The (k, n)-th entry of $\mathbf{W}$ is modeled as

$$(\mathbf{W})_{kn} = \frac{\sqrt{W_R}\ g_{kn}}{4\pi\frac{d_k}{\lambda}\sqrt{k_B T_R B_W}}, \tag{7}$$

where W_R denotes the user receive antennas power gain. g_{kn} is referring to the gain (in power) from feed n toward the k-th user, such that the respective feed transmit gain is $10\log_{10}(|(\mathbf{W})_{kn}|^2)$ if expressed in dBi. Finally, d_k is the distance between the k-th user and the satellite, λ the carrier wavelength, k_B the Boltzmann constant, T_R the receiver noise temperature, and B_W the carrier bandwidth. The reader can refer to [11] for more details about (6).

To mitigate the interference in both UL and FL, we focus exclusively on the linear ZF precoding technique. This technique has been pointed out as an efficient method due to its complete interference rejection capabilities by the pseudoinverse of the channel, while preserving a low computational complexity [14]. To show the impact of precoding on the transmitted data, the vector $\mathbf{x}$ in (5) shall be decomposed as

$$\mathbf{x} = \sqrt{\kappa}\mathbf{T}\mathbf{s}. \tag{8}$$

where $\mathbf{s}$ is the transmit symbol vector and the k-th entry of $\mathbf{s}$ is the constellation symbol destined to the k-th user with $\mathrm{E}\{\mathbf{s}\mathbf{s}^H\} = \mathbf{I}_K$. The matrix $\mathbf{T}$ denotes a $K \times K$ linear ZF precoding matrix. The scalar κ is the power scaling factor and must adapt with

$$\mathrm{trace}(\mathbf{B}\mathbf{T}\mathbf{T}^H\mathbf{B}^H) \leq P, \tag{9}$$

where P is the transmit power of N feeds. Note that the transmit power constraint in (9) is set considering $\mathbf{B}_m$.

Remark 2. Throughout this paper it is conceived that the power allocation mechanism is located at the array fed reflector system with N embedded feeds. ■

B. Signal model in SGN-BMGP and SN-BMGP architectures

Mathematically, the signal model in (5) for SGN-BMGP architecture becomes

$$\mathbf{y} = \mathbf{HBH}_f\mathbf{x}_f + \mathbf{n}, \tag{10}$$

where $\mathbf{H}$ is the UL channel and already discussed before. The matrix $\mathbf{H}_f$ of size $K \times K$ is the FL channel for a given frequency reuse pattern. The vector $\mathbf{x}_f$ in (10) is the transmitted signals at the GWs and decomposed as

$$\mathbf{x}_f = \sqrt{\kappa_f}\mathbf{Ts}, \tag{11}$$

where $\mathbf{s}$ and $\mathbf{T}$ respectively represent transmitted signals at the GWs and precoding scheme which are expressed in (8). For the signal model in (11), the scalar κ_f is the power factor and has to comply with

$$\text{trace}(\mathbf{H}_f\mathbf{BTT}^H\mathbf{B}^H\mathbf{H}_f^H) \leq P. \tag{12}$$

In case of applying SN-BMGP architecture, the signal model in (10) shall be rewritten as

$$\mathbf{y} = \sqrt{\kappa_B}\mathbf{HBH}_f\mathbf{s} + \mathbf{n}, \tag{13}$$

where κ_B has the following constraint

$$\kappa_B = \frac{P}{\text{trace}(\mathbf{BB}^H)}. \tag{14}$$

Next section describes the design of precoding matrix $\mathbf{T}$ and BFN in P-BMGP.

III. P-BMGP ARCHITECTURE

The objective of this section is to provide the design of on-ground ZF precoding $\mathbf{T}$ and on-board BFN $\mathbf{B}$ in a P-BMGP architecture. Recall that, in a P-BMGP network, each GW employs an individual precoder and resulting in a block diagonal $\mathbf{T}$. Moreover, a perfect CSI of all the beams is available at each GW through an error-free CSI feedback role among users and GWs as well as a noiseless CSI exchange mechanism among the GWs. The proposed BFN is also assumed to be fixed and optimized with respect to the UL channel component perturbations.

A. Precoding design in P-BMGP

As stated, we consider the BMGP architecture operates in the cluster mode. A total number of F GWs and clusters are assumed, i.e. one GW per cluster. For instance, m-th ($m = 1, ..., F$) GW serves K_m number of beams/users located in the m-th cluster such that $K = \sum_{m=1}^{F} K_m$. Without loss of generality, we consider an identical number of beams at each cluster, i.e.

$$K_1 = ... = K_m = ... = K_F. \tag{15}$$

The objective of precoding in this context is to mitigate the intra-cluster and inter-cluster interference. The former arises from beams belonging to the same cluster while the latter relates to co-channel interference from beams served from other GWs. For mathematical convenience, we use K_{-m} to denote the number of users located in other cluster different from m with $K_m + K_{-m} = K$ and

$$K_{-1} = ... = K_{-m} = ... = K_{-F}. \tag{16}$$

The notation N_m denotes the number of on-board feeds serving the m-th cluster, with $N = \sum_{m=1}^{F} N_m$. Again, without loss of generality, we let,

$$N_1 = ... = N_m = ... = N_F. \tag{17}$$

The channel matrix $\mathbf{H}$ for a set of F cluster/GWs can be decomposed as

$$\mathbf{H} = (\mathbf{H}_1^R, ..., \mathbf{H}_m^R, ..., \mathbf{H}_F^R), \tag{18}$$

with $\mathbf{H}_m^R$ of size $K \times N_m$ is the channel sub-matrix containing the contribution of the feeds assigned to the m-th GW. Then, we define

$$\mathbf{H}_m \triangleq (\mathbf{H}_m^R)_{K_m \times N_m} \tag{19}$$

as the m-th cluster submatrix obtained by selecting the corresponding $K_m \times N_m$ entries in the matrix $\mathbf{H}_m^R$. Besides,

$$\mathbf{H}_{-m} \triangleq (\mathbf{H}_m^R)_{K_{-m} \times N_m} \tag{20}$$

is the interference posed by the N_m feeds on the adjacent clusters/beams of m. The m-th GW knows the CSI of both $\mathbf{H}_m$ and $\mathbf{H}_{-m}$.

In contrast to the previous works [6],[12], which have not contained a special structure on $\mathbf{B}$, a lower complexity payload is pursued here by operating with a block diagonal $\mathbf{B}$[1]

$$\mathbf{B} = \text{diag}\big(\mathbf{B}_1, ..., \mathbf{B}_m, ..., \mathbf{B}_F\big) \tag{21}$$

where the submatrices $\mathbf{B}_m \triangleq (\mathbf{B})_{N_m \times M_m}, (m = 1, \ldots, F)$ are of size $N_m \times M_m$. The term M_m represents the number of signal streams to be transmitted in the FL from the m-th GW to the satellite, not necessarily equal to N_m, but possibly lower to save bandwidth, and such that $M_m \geq K_m$. For the sake of mathematical clarity, we assume $M_m = K_m$. The BFN transforms the K_m FL signals into N_m feed signals to serve the m-th cluster.

Precoding in (8) is also modeled by a block diagonal matrix,

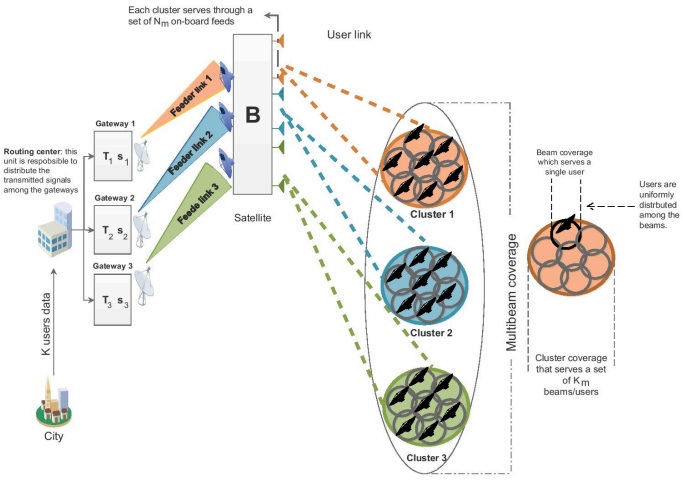

Fig. 1. P-BMGP network for a set of three GWs and clusters.

since each GW can process only its own streams. With this, the signal model in (5) for a set of F GWs is written as

$$\mathbf{y} = \mathbf{HB}\text{diag}\big(\sqrt{\kappa_1}\mathbf{T}_1, ..., \sqrt{\kappa_m}\mathbf{T}_m, ..., \sqrt{\kappa_F}\mathbf{T}_F\big)\mathbf{s} + \mathbf{n} \tag{22}$$

where $\mathbf{y} = \big(\mathbf{y}_1, ..., \mathbf{y}_m, ..., \mathbf{y}_F\big)^T$, $\mathbf{s} = \big(\mathbf{s}_1, ..., \mathbf{s}_m, ..., \mathbf{s}_F\big)^T$, $\mathbf{B}$ is defined in (21) and $\mathbf{T}_m$ of size $K_m \times K_m$ refers to the precoder in the m-th GW. The scalar κ_m is the power scaling factor in the m-th cluster, and has to comply with

$$\kappa_m = \frac{P_m}{\text{trace}\big(\mathbf{B}_m\mathbf{T}_m\mathbf{T}_m^H\mathbf{B}_m^H\big)}, \tag{23}$$

[1]Employing a block diagonal BFN in (21) instead of the proposed BFN in [6] and [12] establishes an affordable payload complexity through enforcing off-block diagonal elements of $\mathbf{B}$ to be zero (with no required processing in zero elements).

with P_m denoting the total transmit power of N_m feeds.
As an example, the signal model in (22) for three GWs and clusters can be expressed as follows

$$\underbrace{\begin{pmatrix}\mathbf{y}_1\\ \mathbf{y}_2\\ \mathbf{y}_3\end{pmatrix}}_{\mathbf{y}}=\underbrace{\begin{pmatrix}(\mathbf{H})_1 & (\mathbf{H})_{12} & (\mathbf{H})_{13}\\ (\mathbf{H})_{21} & (\mathbf{H})_2 & (\mathbf{H})_{23}\\ (\mathbf{H})_{31} & (\mathbf{H})_{32} & (\mathbf{H})_3\end{pmatrix}}_{\mathbf{H}}\underbrace{\begin{pmatrix}\mathbf{B}_1 & 0 & 0\\ 0 & \mathbf{B}_2 & 0\\ 0 & 0 & \mathbf{B}_3\end{pmatrix}}_{\mathbf{B}}\underbrace{\begin{pmatrix}\sqrt{\kappa_1}\mathbf{T}_1 & 0 & 0\\ 0 & \sqrt{\kappa_2}\mathbf{T}_2 & 0\\ 0 & 0 & \sqrt{\kappa_3}\mathbf{T}_3\end{pmatrix}}_{\mathbf{T}}\underbrace{\begin{pmatrix}\mathbf{s}_1\\ \mathbf{s}_2\\ \mathbf{s}_3\end{pmatrix}}_{\mathbf{s}}+\underbrace{\begin{pmatrix}\mathbf{n}_1\\ \mathbf{n}_2\\ \mathbf{n}_3\end{pmatrix}}_{\mathbf{n}}, \tag{24}$$

where $\mathbf{H}_{-1} \triangleq \binom{(\mathbf{H})_{21}}{(\mathbf{H})_{31}}$, $\mathbf{H}_{-2} \triangleq \binom{(\mathbf{H})_{12}}{(\mathbf{H})_{32}}$ and $\mathbf{H}_{-3} \triangleq \binom{(\mathbf{H})_{13}}{(\mathbf{H})_{23}}$.
For mathematical convenience, we also define $\mathbf{H}_m \triangleq (\mathbf{H})_m$; and $\mathbf{H}_{mi} \triangleq (\mathbf{H})_{mi}$ which denotes the interference received by the m-th cluster from the i-th cluster, with $m \neq i$ and $i = 1, ..., (F-1)$. For the sake of clarity, Figure 1 depicts a multibeam communication infrastructure with three GWs as modeled in (24).
In this context, the signal model in (24) for the m-th cluster is written as

$$\mathbf{y}_m = \sqrt{\kappa_m}\mathbf{H}_m\mathbf{B}_m\mathbf{T}_m\mathbf{s}_m + \sqrt{\kappa_i}\sum_{m\neq i}^{F-1}\mathbf{H}_{mi}\mathbf{B}_i\mathbf{T}_i\mathbf{s}_i + \mathbf{n}_m, \tag{25}$$

and the Signal to Noise plus Interference Ratio (SINR) of the m-th cluster is obtained by

$$\text{SINR}_m = \frac{\kappa_m \text{trace}(\mathbf{H}_m\mathbf{B}_m\mathbf{T}_m\mathbf{T}_m^H\mathbf{B}_m^H\mathbf{H}_m^H)}{\kappa_i\sum_{i\neq m}\text{trace}(\mathbf{H}_{mi}\mathbf{B}_i\mathbf{T}_i\mathbf{T}_i^H\mathbf{B}_i^H\mathbf{H}_{mi}^H)+1}. \tag{26}$$

Then, the underlying problem for the m-th cluster can be formulated as

$$\begin{aligned}\max_{\mathbf{T}_m,\mathbf{B}_m}\quad & \text{SINR}_m \\ s.t.\quad & \text{trace}\big(\mathbf{B}_m\mathbf{T}_m\mathbf{T}_m^H\mathbf{B}_m^H\big) \leq P_m.\end{aligned} \tag{27}$$

To maximize SINR_m in (27), the promising solution would be jointly design the matrices $\mathbf{B}_m$ and $\mathbf{T}_m$, which guarantees:
Requirements.1. Nulling the inter-cluster interference through designing the precoding scheme $\mathbf{T}_m$ and obtains $\text{trace}(\mathbf{H}_{mi}\mathbf{B}_i\mathbf{T}_i\mathbf{T}_i^H\mathbf{B}_i^H\mathbf{H}_{mi}^H) = diag(\tau)$, where

$$\tau \triangleq arg\ min\big\{\text{trace}(\mathbf{H}_{mi}\mathbf{B}_i\mathbf{T}_i\mathbf{T}_i^H\mathbf{B}_i^H\mathbf{H}_{mi}^H)\big\}.$$

Requirements.2. Nulling the intra-cluster interference in addition to inter-cluster interference through the design of $\mathbf{T}_m$ and establishes $diag\big\{\text{trace}(\mathbf{H}_m\mathbf{B}_m\mathbf{T}_m\mathbf{T}_m^H\mathbf{B}_m^H\mathbf{H}_m^H)\big\}$.
Requirements.3. Optimizing the power loading factor κ_m in (23) and obtains $arg\ min\big\{\text{trace}\big(\mathbf{B}_m\mathbf{T}_m\mathbf{T}_m^H\mathbf{B}_m^H\big)\big\}$, which is exploited through employing the joint design of $\mathbf{T}_m$ and $\mathbf{B}_m$. Note that only optimizing Requirements.3 is performed at the payload aiming at preserving low computationally complex.
For a moment, let us consider the satellite payload works in the transparent mode, i.e. $\mathbf{B} = \mathbf{I}_N$, and the signal processing scheme is only done at the ground segment (i.e. at the GW) such that the $\mathbf{T}_m$ precodes direcly a set of K_m user signal into N_m FL signals for the m-th cluster. In such a configuration, a promising block ZF precoding scheme to cope with inter- and intra-cluster interference is given by [15]

$$\mathbf{T}_m = \mathbf{Q}_m^H\big(\mathbf{Q}_m\mathbf{Q}_m^H\big)^{-1} \tag{28}$$

where

$$\mathbf{Q}_m \triangleq \mathbf{H}_m\mathbf{V}_{-m}^0\mathbf{V}_{-m}^{0,H}. \tag{29}$$

We write the Singular Value Decomposition (SVD) for the inter-cluster interfering channel as

$$\mathbf{H}_{-m} = \mathbf{U}_{-m}\mathbf{\Sigma}_{-m}\mathbf{V}_{-m}^H, \tag{30}$$

with the matrix $\mathbf{V}_{-m}^0$ refers to the last $(N_m - K_{-m})$ columns of matrix $\mathbf{V}_{-m}$ and denotes the null space of $\mathbf{H}_{-m}$. The power operator κ_m in (23) for the proposed precoding scheme in (28) is obtained by

$$\kappa_{p,m} = \frac{P_m}{\text{trace}\big(\mathbf{T}_m\mathbf{T}_m^H\big)} = \frac{P_m}{\text{trace}\big((\mathbf{Q}_m\mathbf{Q}_m^H)^{-1}\big)}. \tag{31}$$

Obviously, the proposed $\mathbf{T}_m$ in (28) fulfills the Requirements 1-3 and the SINR_m in (26) becomes

$$\text{SINR}_m = \kappa_{p,m}. \tag{32}$$

Note that the sufficient condition for obtaining $\mathbf{V}_{-m}^0$ in (30) is to have $K_{-m} < N_m$.
Unfortunately, in case of $K_{-m} > N_m$, the null space matrix $\mathbf{V}_{-m}^0$ is empty. To cope with this circumstance, we propose the following design of $\mathbf{T}_m$:

$$\mathbf{T}_m = \mathbf{Q}_{r,m}^H\big(\mathbf{Q}_{r,m}\mathbf{Q}_{r,m}^H\big)^{-1} \tag{33}$$

with

$$\mathbf{Q}_{r,m} \triangleq \mathbf{H}_{r,m}\mathbf{V}_{r,-m}^0\mathbf{V}_{r,-m}^{0,H}\mathbf{R}_m, \tag{34}$$

and $\mathbf{R}_m = \binom{(\mathbf{I})_{N_m\times N_m}}{(\mathbf{I})_{K_{-m}\times N_m}}$.
For (33), the matrix $\mathbf{H}_{r,m}$ is the rescaled version of $\mathbf{H}_m$ and can be defined by $\mathbf{H}_{r,m} = \mathbf{H}_m\mathbf{R}_m^H$. Moreover, with the SVD of $\mathbf{H}_{-m}\mathbf{R}_m^H = \mathbf{U}_{r,-m}\mathbf{\Sigma}_{r,-m}\mathbf{V}_{r,-m}^H$, the matrix $\mathbf{V}_{r,-m}^0$ refers to the null space of $(\mathbf{H}_{-m}\mathbf{R}_m^H)$. The reader can refer to [9] and [16] for more methodologies to find the null space of a matrix in case of $K_{-m} > N_m$.
It is worth to note here that the rest of the analytic analysis of this section is developed taking into account $K_{-m} < N_m$ degree of freedom at the payload. The sketch of the system analyzing with $K_{-m} > N_m$ is similar by adding a rescaling identity matrix $\mathbf{R}_m$. In addition, for the case $K_{-m} < N_m$, a sufficient condition is having at least $N_m \geq K_{-m}$ for inter-cluster and $N_m \geq K_{-m} + K_m$ for intra-cluster when K_m is the same for all GWs, then $K_{-m} = (F-1)K_m$ feeds at the m-th cluster. An increase in the number of users results in an unrealistic payload structure due to the required large number of feeds. Thus, the number of users per cluster should be properly selected with respect to the number of available feeds per cluster.
In the presence of on-board BFN, the earlier results hold when $\mathbf{T}_m$ is replaced by $\mathbf{B}_m\mathbf{T}_m$. Further, we see that, it is possible to let $\mathbf{T}_m$ have the dimension of $K_m \times K_m$ and $\mathbf{B}_m$ to be $N_m \times K_m$. In that sense, we have,

$$\mathbf{B}_m\mathbf{T}_m \rightarrow \mathbf{B}_m\mathbf{T}_m = \mathbf{Q}_m^H(\mathbf{Q}_m\mathbf{Q}_m^H)^{-1}. \tag{35}$$

Employing $(\mathbf{B}_m^H\mathbf{B}_m)^{-1}\mathbf{B}_m^H$ at the both sides of (38) holds

$$\mathbf{T}_m = (\mathbf{B}_m^H\mathbf{B}_m)^{-1}\mathbf{B}_m^H\mathbf{Q}_m^H(\mathbf{Q}_m\mathbf{Q}_m^H)^{-1}. \tag{36}$$

To find an optimal design of BFN, we restrict the $\mathbf{B}_m$ in (36) to be

$$\mathbf{B}_m^H\mathbf{B}_m = \mathbf{I}_{K_m}, \tag{37}$$

where this implies on-board BFN is constructed with orthonormal vectors. Given (37), the precoding in (35) is rewritten as

$$\mathbf{T}_m = \mathbf{B}_m^H\mathbf{Q}_m^H(\mathbf{Q}_m\mathbf{Q}_m^H)^{-1}. \tag{38}$$

The scalar κ_m in (23) with the formulation of precoding in (38) as well as the assumption in (37) is recalculated as

$$\kappa_m = \frac{P_m}{\text{trace}\,(\mathbf{B}_m^H\mathbf{Q}_m^H(\mathbf{Q}_m\mathbf{Q}_m^H)^{-2}\mathbf{Q}_m\mathbf{B}_m)}. \tag{39}$$

Let us consider the SVD of $\mathbf{Q}_m = \mathbf{U}_m\mathbf{\Sigma}_m\mathbf{V}_m^H$. Then, an optimal $\mathbf{B}_m$ can be constructed through the following matrices

$$\mathbf{B}_m^\star = \mathbf{V}_{-m}^0\begin{pmatrix}\mathbf{U}_m\\ \mathbf{z}\end{pmatrix} \qquad m = 1, \ldots, F \tag{40}$$

where $\mathbf{z}$ of size $\big((N_m - K_{-m}) - K_m \times K_m\big)$ is a zero matrix. With applying $\mathbf{B}_m^\star$ in (40), the Requirements.1-3 are satisfied

and the SINR_m in (26) becomes

$$\text{SINR}_m = \kappa_{p,m} = \frac{P_m}{\text{trace}\left(\mathbf{B}_m^{\star,H}\mathbf{Q}_m^H(\mathbf{Q}_m\mathbf{Q}_m^H)^{-2}\mathbf{Q}_m\mathbf{B}_m^{\star}\right)} = \frac{P_m}{\text{trace}\big((\mathbf{Q}_m\mathbf{Q}_m^H)^{-1}\big)}, \tag{41}$$

where

$$\text{trace}\left(\mathbf{B}_m^H\mathbf{Q}_m^H(\mathbf{Q}_m\mathbf{Q}_m^H)^{-2}\mathbf{Q}_m\mathbf{B}_m\right) \geq \text{trace}\left(\mathbf{B}_m^{\star,H}\mathbf{Q}_m^H(\mathbf{Q}_m\mathbf{Q}_m^H)^{-2}\mathbf{Q}_m\mathbf{B}_m^{\star}\right) = \text{trace}\big((\mathbf{Q}_m\mathbf{Q}_m^H)^{-1}\big). \tag{42}$$

Proof. For the proof of inequality in (42), see Appendix A. ■

However, while the UL channel varies, the optimal $\mathbf{B}_m$ in (40) should adapt with the UL channel variation, leading to a large complexity at the payload. Even though the UL channel appears to be variable, next section aims at finding the best possible fixed design of $\mathbf{B}_m$ with respect to the UL channel perturbation.

Consequently, the constructing fixed $\mathbf{B}_m$ includes the following steps:

(a) We begin by designing a fixed $\mathbf{B}_m$ which optimizes the power factor κ_m in the calculated SINR_m (27) and fulfills the Requirements 3. To this end, for the κ_m in (39), the objective problem can be formulated as

$$\min_{\mathbf{B}_m} \quad \text{trace}\left(\mathbf{B}_m^H\mathbf{Q}_m^H(\mathbf{Q}_m\mathbf{Q}_m^H)^{-2}\mathbf{Q}_m\mathbf{B}_m\right) \qquad s.t. \quad \mathbf{B}_m^H\mathbf{B}_m = \mathbf{I}_{K_m}. \tag{43}$$

(b) We show that the obtained $\mathbf{B}_m$ in (a) fulfills Requirements 1- 2.

B. Fixed BFN design in P-BMGP

Towards generating a fixed BFN, we consider the channel matrix $\mathbf{H}_m$ for the m-th GW can be decomposed as [17]

$$\mathbf{H}_m = \hat{\mathbf{H}}_m + \mathbf{\Delta H}_m, \tag{44}$$

where $\hat{\mathbf{H}}_m$ represents the mean channel response with respect to random user locations[2] of $\mathbf{H}_m$. Perturbation matrix $\mathbf{\Delta H}_m$ models the difference between the actual value and its mean. Similarly, we formulate a perturbation model for the null subspace in (30):

$$\mathbf{V}_{-m}^0 = \hat{\mathbf{V}}_{-m}^0 + \mathbf{\Delta V}_{-m}^0. \tag{45}$$

We assume that the actual matrices $\mathbf{H}_m$ and $\mathbf{V}_{-m}^0$ respectively relay on the neighborhood of the nominal channel matrices $\hat{\mathbf{H}}_m$ and $\hat{\mathbf{V}}_{-m}^0$ that are known to the m-th GW. In particular, we consider that $\mathbf{H}_m$ and $\hat{\mathbf{V}}_{-m}^0$ respectively belong to the uncertainty regions

$$\mathcal{H}_m = \{||\mathbf{H}_m - \hat{\mathbf{H}}_m|| \leq \alpha_{\mathbf{\Delta H}_m}\} \tag{46}$$

and

$$\mathcal{V}_m = \{||\mathbf{V}_{-m}^0 - \hat{\mathbf{V}}_{-m}^0|| \leq \alpha_{\mathbf{\Delta V}_{-m}^0}\}, \tag{47}$$

which are two spheres centered at $\alpha_{\mathbf{\Delta H}_m}$ and $\alpha_{\mathbf{\Delta V}_{-m}^0}$.

Interestingly, the channel model in (44) and (45) resembles the modeling of a MIMO system with imperfect CSI at the transmitter which has been solved as a worst case optimization problem in [18]-[20]. With this perspective, the worst case robust design is considered, which leads to a maxmin or minmax formulation. The corresponding minmax problem for the m-th cluster is intended to maximize the minimum of the trace $\left(\mathbf{B}_m^H\mathbf{Q}_m^H(\mathbf{Q}_m\mathbf{Q}_m^H)^{-2}\mathbf{Q}_m\mathbf{B}_m\right)$ in (43), i.e,

$$\min_{\mathbf{B}_m} \quad \max_{\mathbf{\Delta H}_m, \mathbf{\Delta V}_{-m}^0} \quad \text{trace}\left(\mathbf{B}_m^H\mathbf{Q}_m^H(\mathbf{Q}_m\mathbf{Q}_m^H)^{-2}\mathbf{Q}_m\mathbf{B}_m\right) \qquad s.t. \quad \mathbf{B}_m^H\mathbf{B}_m = \mathbf{I}_{K_m}. \tag{48}$$

[2]Other random fluctuations are expected, even for fixed users, such as phase noise.

Theorem 1. *The derivation of the solution for* (48) *goes along the following logic:*

(i) *We set upper bounds $\alpha_{\mathbf{\Delta H}_m}$ and $\alpha_{\mathbf{\Delta V}_{-m}^0}$ for the spectral norms $||\mathbf{\Delta H}_m||$ (i.e. $||\mathbf{\Delta H}_m|| \leq \alpha_{\mathbf{\Delta H}_m}$) and $||\mathbf{\Delta V}_{-m}^0||$ (i.e. $||\mathbf{\Delta V}_{-m}^0|| \leq \alpha_{\mathbf{\Delta V}_{-m}^0}$), respectively.*

(ii) *An upper bound $\mathbf{Q}_m^H(\mathbf{Q}_m\mathbf{Q}_m^H)^{-2}\mathbf{Q}_m \leq \breve{\mathbf{S}}_m$ is found leading to trace $\left(\mathbf{B}_m^H\mathbf{Q}_m^H(\mathbf{Q}_m\mathbf{Q}_m^H)^{-2}\mathbf{Q}_m\mathbf{B}_m\right) \leq$ trace $\left(\mathbf{B}_m^H\breve{\mathbf{S}}_m\mathbf{B}_m\right)$. Note that $\breve{\mathbf{S}}_m$ is the upper bound of $\mathbf{Q}_m^H(\mathbf{Q}_m\mathbf{Q}_m^H)^{-2}\mathbf{Q}_m$.*

(iii) *With considering SVD of $\breve{\mathbf{S}}_m = \breve{\mathbf{L}}_m\breve{\mathbf{\Omega}}_m\breve{\mathbf{L}}_m^H$ and $\hat{\mathbf{H}}_m\hat{\mathbf{H}}_m^H = \mathbf{U}_{H,m}\mathbf{\Sigma}_{H,m}\mathbf{U}_{H,m}^H$, it can be shown that*

$$\mathbf{B}_m = \breve{\mathbf{L}}_m\begin{pmatrix}\mathbf{U}_{H,m}\\ \mathbf{w}\end{pmatrix} \tag{49}$$

maximizes the minimum of the objective problem in (48)*. The matrix $\mathbf{w}$ of size $(N_m - K_m) \times K_m$ is a zero matrix.*

Proof. For the proof of Theorem 1, see Appendix B. ■

Indeed, the proposed fixed $\mathbf{B}_m$ in (49) supports Requirements 1- 3 and, similar to the $\mathbf{B}_m$ (40), the SINR_m in (27) becomes $\text{SINR}_m = \kappa_{p,m}$.

Having solved the case without GW interference, we now proceed to the SGN-BMGP.

IV. SGN-BMGP ARCHITECTURE

This section involves with developing space and ground segments for a SGN-BMGP architecture. Designing the BMGP architecture in Section III has been based on the fact that the GWs are able to transmit the feed signals within several interference-free and noiseless FLs (i.e. one FL per GW) to the satellite. As a matter of fact, considering noiseless and interference-free FL would be a naive approach and consequently, an additional inter FLs interference shall be taken into account in developing the BMGP networks.

The mathematical signal model of the SGN-BMGP architecture is already introduced in (10). Analogous to the UL channel decomposition in (18), for a set of F cluster/GWs, we consider

$$\mathbf{H}_f = (\mathbf{H}_{f,1}^R, ..., \mathbf{H}_{f,m}^R, ..., \mathbf{H}_{f,F}^R), \tag{50}$$

with $\mathbf{H}_{f,m}^R$ of size $K \times K_m$ to be the channel sub-matrix containing the contribution of the feeds assigned to the m-th GW. Also, we define

$$\mathbf{H}_{f,m} \triangleq (\mathbf{H}_{f,m}^R)_{K_m \times K_m} \tag{51}$$

as the m-th GW submatrix obtained by selecting the corresponding $K_m \times K_m$ entries in the matrix $\mathbf{H}_{f,m}^R$. The interference posed by the K_{-m} feeds on adjacent GWs is characterized by submatrix $\mathbf{H}_{f,-m}$ and defined as

$$\mathbf{H}_{f,-m} \triangleq (\mathbf{H}_{f,m}^R)_{K_{-m} \times K_m}. \tag{52}$$

We assume that the m-th GW knows both $\mathbf{H}_{f,m}$ and $\mathbf{H}_{f,-m}$ through a noiseless CSI exchange network among the GWs.

Now, the objective is to design the precoding matrix $\mathbf{T}_m$ and $\mathbf{B}_m$ for the m-th GW aiming at minimizing the inter-cluster, intra-cluster and inter-FL interference. In general, our main approach in this context goes along the following logic: First, the $\mathbf{T}_m$ matrix is designed in order to tackle with the inter-FL interference through an appropriate ZF scheme. Second, the BFN is constructed to minimize the inter- and intra-cluster

interference in the UL. We also expect that the precoding matrix, in addition to rejecting the inter-FL interference, can help the on-board BFN with slightly mitigating interference in the UL. Indeed, the on-board BFN only equalizes partially inter- and intra-cluster interference, leading to a low computationally complex payload architecture.

A. Precoding design in SGN-BMGP

To mitigate the inter-FL interference through $\mathbf{T}_m$, we propose the following configuration of ZF precoding scheme:

$$\mathbf{T}_m = \mathbf{Q}_{f,m}^H(\mathbf{Q}_{f,m}\mathbf{Q}_{f,m}^H)^{-1}, \tag{53}$$

with

$$\mathbf{Q}_{f,m} \triangleq \mathbf{H}_{f,m}\mathbf{R}_{f,m}^H\mathbf{V}_{f,m}^0\mathbf{V}_{f,m}^{0,H}\mathbf{R}_{f,m}, \tag{54}$$

where $\mathbf{R}_{f,m} = \begin{pmatrix}(\mathbf{I})_{K_m\times K_m}\\ (\mathbf{I})_{K_{-m}\times K_m}\end{pmatrix}$. Using the SVD of $\mathbf{H}_{f,-m}\mathbf{R}_{f,m}^H = \mathbf{U}_{f,m}\mathbf{\Sigma}_{f,m}\mathbf{V}_{f,m}^H$, the matrix $\mathbf{V}_{f,m}^0$ refers to the null space of $(\mathbf{H}_{f,-m}\mathbf{R}_{f,m}^H)$.

With (53), the received signal for the m-th cluster becomes similar to the signal received (25) at the P-BMGP architecture. Interestingly, designing a simple UL channel adaptive BFN in (25) can be also analogous to the obtained ZF precoding designs in (28), i.e. $\mathbf{B}_m = \mathbf{Q}_m^H(\mathbf{Q}_m\mathbf{Q}_m^H)^{-1}$, and (33), i.e. $\mathbf{B}_m = \mathbf{Q}_{r,m}^H(\mathbf{Q}_{r,m}\mathbf{Q}_{r,m}^H)^{-1}$, for the cases of $K_{-m} \leq N_m$ and $K_{-m} \geq N_m$, respectively. However, these schemes suffer from high complexities due to the variation of channel components employed in $\mathbf{Q}_m$ and $\mathbf{Q}_{r,m}$.

Next section aims to obtain a fixed $\mathbf{B}_m$ which provides a good trade off between complexity and performance.

B. Fixed BFN design in SGN-BMGP

As stated above, to design fixed BFN, we presume the precoding matrix has two roles. First, it minimizes the impact of the inter-FL interference as already computed in (53). Then, the precoder partially mitigates the inter-cluster and intra-cluster interference. To this end, the precoding matrix $\mathbf{T}_m$ shall be decomposed as

$$\mathbf{T}_m = \mathbf{T}_{m,a}\mathbf{T}_{m,b}, \tag{55}$$

where $\mathbf{T}_{m,a} = \mathbf{Q}_{f,m}^H(\mathbf{Q}_{f,m}\mathbf{Q}_{f,m}^H)^{-1}$ is used to minimize the inter-FL interference. The matrix $\mathbf{T}_{m,b}$ is aimed at partially rejecting the inter-cluster and intra-cluster interference. For computing $\mathbf{T}_{m,b}$ and $\mathbf{B}_m$, we use Mean Square Error (MSE) performance metric which is realized for the m-th GW as

$$\mathbf{MSE}_m = \mathrm{E}\{(\mathbf{s}_m - \hat{\mathbf{s}}_m)(\mathbf{s}_m - \hat{\mathbf{s}}_m)^H\}, \tag{56}$$

where $\hat{\mathbf{s}}_m = (\sqrt{\kappa_m})^{-1}\mathbf{y}_m$ and the calculation of vector $\mathbf{y}_m$ is expressed in (25). In this context, the Sum MSE (SMSE) can be written as

$$\text{SMSE} = \sum_{m=1}^{F}\text{trace}(\mathbf{MSE}_m) = \sum_{m=1}^{F}\text{trace}\left(\mathrm{E}\{(\mathbf{s}_m - \hat{\mathbf{s}}_m)(\mathbf{s}_m - \hat{\mathbf{s}}_m)^H\}\right). \tag{57}$$

The objective problem to minimize SMSE in (57) can be formulated as

$$\begin{aligned}\min_{\mathbf{B}_m,\mathbf{T}_m}\quad & \text{trace}\left(\mathrm{E}\{(\mathbf{s}_m - \hat{\mathbf{s}}_m)(\mathbf{s}_m - \hat{\mathbf{s}}_m)^H\}\right)\\ s.t.\quad & \mathbf{B}_m^H\mathbf{B}_m = \mathbf{I}_{K_m}.\end{aligned} \tag{58}$$

Given (25) and (55), the SMSE for a set of F GWs is obtained as

$$\text{SMSE} = \sum_{m=1}^{F}\text{trace}(\mathbf{MSE}_m) = \sum_{m}^{F}\text{trace}\Big\{\mathbf{I}_{K_m} - \frac{1}{\sqrt{\kappa_m}}(\mathbf{H}_m\mathbf{B}_m\mathbf{T}_{m,b} + \mathbf{T}_{m,b}^H\mathbf{B}_m^H\mathbf{H}_m^H) + \frac{1}{\kappa_m}\mathbf{T}_{m,b}^H\left(\mathbf{B}_m^H\mathbf{H}_m^H\mathbf{H}_m\mathbf{B}_m + \mathbf{B}_m^H(\sum_{i\neq m}\frac{\kappa_m}{\kappa_i}\mathbf{H}_{mi}^H\mathbf{H}_{mi})\mathbf{B}_m\right)\mathbf{T}_{m,b} + \frac{1}{\kappa_m}\mathbf{I}_{K_m}\Big\}. \tag{59}$$

Then, the optimal design of $\mathbf{T}_{m,b}$ can be calculated as

$$\frac{\partial\text{SMSE}}{\partial\mathbf{T}_{m,b}} = 0 \rightarrow \mathbf{T}_{m,b} = \left(\mathbf{B}_m^H\mathbf{H}_m^H\mathbf{H}_m\mathbf{B}_m + \mathbf{B}_m^H(\sum_{i\neq m}\frac{\kappa_m}{\kappa_i}\mathbf{H}_{mi}^H\mathbf{H}_{mi})\mathbf{B}_m\right)^{-1}\mathbf{B}_m^H\mathbf{H}_m^H, \tag{60}$$

which optimizes the SMSE in (59) to [3]

$$\text{SMSE} = \sum_{m}^{F}\text{trace}\Big\{\mathbf{I}_{K_m} - \mathbf{H}_m\mathbf{B}_m\left(\mathbf{B}_m^H\mathbf{H}_m^H\mathbf{H}_m\mathbf{B}_m + \mathbf{B}_m^H(\sum_{i\neq m}\frac{\kappa_m}{\kappa_i}\mathbf{H}_{mi}^H\mathbf{H}_{mi})\mathbf{B}_m\right)^{-1}\mathbf{B}_m^H\mathbf{H}_m^H + \frac{1}{\kappa_m}\mathbf{I}_{K_m}\Big\}. \tag{61}$$

Note that the matrix $\mathbf{T}_{m,b}$ in (60) is a ZF precoding scheme with an additional regularized factor $\mathbf{B}_m^H(\sum_{i\neq m}\frac{\kappa_m}{\kappa_i}\mathbf{H}_{mi}^H\mathbf{H}_{mi})^{-1}\mathbf{B}_m$.

To find fixed $\mathbf{B}_m$ in (61), we use the minmax analyzing which is already discussed in Section III.B. In this context, denoting

$$\mathbf{H}_{mi} = \hat{\mathbf{H}}_{mi} + \mathbf{\Delta H}_{mi}, \tag{62}$$

where $\hat{\mathbf{H}}_{mi}$ and $\mathbf{\Delta H}_{mi}$ are respectively the mean and perturbation matrices of $\mathbf{H}_{mi}$ with $||\mathbf{\Delta H}_{mi}|| \leq \alpha_{\mathbf{\Delta H}_{mi}}$, the objective problem can be formulated as

$$\begin{aligned}\min_{\mathbf{B}_m}\ \max_{\mathbf{\Delta H}_m,\mathbf{\Delta H}_{mi}}\quad & \text{trace}\Big\{\left(\mathbf{B}_m^H\mathbf{H}_m^H\mathbf{H}_m\mathbf{B}_m + \mathbf{B}_m^H(\sum_{i\neq m}\frac{\kappa_m}{\kappa_i}\mathbf{H}_{mi}^H\mathbf{H}_{mi})\mathbf{B}_m\right)^{-1}\mathbf{B}_m^H\mathbf{H}_m^H\mathbf{H}_m\mathbf{B}_m\Big\}\\ s.t.\quad & \mathbf{B}_m^H\mathbf{B}_m = \mathbf{I}_{K_m}\\ & \mathbf{H}_m = \hat{\mathbf{H}}_m + \mathbf{\Delta H}_m\\ & \mathbf{H}_{mi} = \hat{\mathbf{H}}_{mi} + \mathbf{\Delta H}_{mi}.\end{aligned} \tag{63}$$

Theorem 2. *Let us define* $\epsilon_f \triangleq 2\alpha_{\mathbf{\Delta H}_{mi}}\sigma_{max}(\hat{\mathbf{H}}_{mi}^H) + \alpha_{\mathbf{\Delta H}_{mi}}^2$ *and* $\breve{\mathbf{M}}_m \triangleq \left((\sum_{i\neq m}\frac{\kappa_m}{\kappa_i}\lambda_{max}(\hat{\mathbf{H}}_{mi}\hat{\mathbf{H}}_{mi}^H) - \epsilon_f)^+) + (\lambda_{max}(\hat{\mathbf{H}}_m\hat{\mathbf{H}}_m^H) - \epsilon_H)^+\right)^{-1}\mathbf{U}_{H,m}(\mathbf{\Sigma}_{H,m} + \epsilon_H\mathbf{I}_{K_m})\mathbf{U}_{H,m}$.

Then, with SVD of $\breve{\mathbf{M}}_m = \breve{\mathbf{S}}_m\breve{\mathbf{\Psi}}_m\breve{\mathbf{S}}_m^H$, *the optimal design of* $\mathbf{B}_m$ *in* (63) *is obtained as*

$$\mathbf{B}_m^\star = \breve{\mathbf{S}}_m\begin{pmatrix}\mathbf{U}_{H,m}\\ \mathbf{w}\end{pmatrix}\qquad, m = 1,\ldots,F \tag{64}$$

where $\mathbf{w}$ *of size* $(N_m - K_m)\times K_m$ *is a zero matrix.*

Proof. For the proof of Theorem 2, see Appendix C. ■

Let us now proceed with analyzing SN-BMGP architecture.

V. SN-BMGP ARCHITECTURE

This section provides analyzing the SN-BMGP networks. We present here a joint design of ZF precoding and BFN at the payload of a BMGP architecture aiming at managing both FL and UL channels interference. The signal model of SN-BMGP architecture is already expressed in (13).

To design $\mathbf{B}$, we propose the following decomposition

$$\mathbf{B} = \mathbf{B}_a\mathbf{B}_b, \tag{65}$$

where $\mathbf{B}_a$ of size $N\times K$ and $\mathbf{B}_b$ of size $K\times K$ are employed to equalize the impact of UL channel $\mathbf{H}$ and FL $\mathbf{H}_f$, respectively. Applying $\hat{\mathbf{s}} = (\sqrt{\kappa}_B)^{-1}\mathbf{y}$ in (13), the performance metric SMSE for the signal model in (13) is calculated as

[3] For arbitrary matrices $\mathbf{A}$, $\mathbf{B}$ and $\mathbf{C}$ we have [21]: $(\mathbf{A}+\mathbf{BC})^{-1} = \mathbf{A}^{-1} - \mathbf{A}^{-1}\mathbf{B}(\mathbf{I}+\mathbf{CA}^{-1}\mathbf{B})^{-1}\mathbf{CA}^{-1}$

$$\text{SMSE} = \text{trace}\left(\text{E}\{(\mathbf{s}-\hat{\mathbf{s}})(\mathbf{s}-\hat{\mathbf{s}})^H\}\right) = \text{trace}\{ (\mathbf{HB}_a\mathbf{B}_b\mathbf{H}_f\mathbf{s}+(\sqrt{\kappa}_B)^{-1}\mathbf{n}-\mathbf{s})(\mathbf{HB}_a\mathbf{B}_b\mathbf{H}_f\mathbf{s}+(\sqrt{\kappa}_B)^{-1}\mathbf{n}-\mathbf{s})^H\}. \quad (66)$$

As an initial approach, the channel adaptive design of $\mathbf{B}_a$ and $\mathbf{B}_b$ which optimize the SMSE in (66) can be easily presented as

$$\frac{\partial \text{SMSE}}{\partial \mathbf{B}_a} = 0 \rightarrow \mathbf{B}_a = \mathbf{H}^H(\mathbf{H}\mathbf{H}^H)^{-1}, \quad (67)$$

$$\frac{\partial \text{SMSE}}{\partial \mathbf{B}_b} = 0 \rightarrow \mathbf{B}_b = \mathbf{H}_f^H(\mathbf{H}_f\mathbf{H}_f^H)^{-1}. \quad (68)$$

To keep complexity low at the payload, the rest of this section provides fixed design $\mathbf{B}_a$ and $\mathbf{B}_b$.

For this, we use again the minmax formulation on the objective problem in (66) which is widely used in the previous sections, i.e,

$$\min_{\mathbf{B}} \max_{\mathbf{\Delta H},\mathbf{\Delta H}_f} \text{trace}\{(\mathbf{HBH}_f\mathbf{s}+(\sqrt{\kappa}_B)^{-1}\mathbf{n}-\mathbf{s})(\mathbf{HBH}_f\mathbf{s}+(\sqrt{\kappa}_B)^{-1}\mathbf{n}-\mathbf{s})^H\} \quad s.t. \quad \mathbf{H}=\hat{\mathbf{H}}+\mathbf{\Delta H},\ \mathbf{H}_f=\hat{\mathbf{H}}_f+\mathbf{\Delta H}_f,\ \text{trace}(\mathbf{BB}^H)\le P, \quad (69)$$

where the decomposition of $\mathbf{H}$ is presented in (44) with considering the whole coverage area and neglecting the index m as well as $||\mathbf{\Delta H}|| \le \alpha_{\mathbf{\Delta H}}$. For $\mathbf{H}_f = \hat{\mathbf{H}}_f + \mathbf{\Delta H}_f$, the matrices $\hat{\mathbf{H}}_f$ and $\mathbf{\Delta H}_f$ denote respectively the mean and perturbation of $\mathbf{H}_f$ such that $||\mathbf{\Delta H}_f|| \le \alpha_{\mathbf{\Delta H}_f}$.

With employing Lemma 7.3 in [22] and applying some mathematical manipulation, the SMSE in (69) is upper bounded by

$$\text{SMSE} \le \widetilde{\text{SMSE}} \triangleq \text{trace}\big[-\hat{\mathbf{H}}\mathbf{B}_a\mathbf{B}_b\hat{\mathbf{H}}_f-\hat{\mathbf{H}}_f^H\mathbf{B}_b^H\mathbf{B}_a^H\hat{\mathbf{H}}^H+\frac{1}{\kappa_B}\mathbf{I}_K + \mathbf{B}_b^H\mathbf{B}_a^H(\hat{\mathbf{H}}^H\hat{\mathbf{H}}+\varphi_H\mathbf{I}_N)\mathbf{B}_a\mathbf{B}_b(\hat{\mathbf{H}}_f\hat{\mathbf{H}}_f^H+\varphi_f\mathbf{I}_K)-2 \big(\alpha_{\mathbf{\Delta H}}\alpha_{\mathbf{\Delta H}_f}-\alpha_{\mathbf{\Delta H}_f}\sigma_{\max}(\hat{\mathbf{H}})-\alpha_{\mathbf{\Delta H}}\sigma_{\max}(\hat{\mathbf{H}}_f)\big)\mathbf{B}_b^H\mathbf{B}_a^H\mathbf{B}_a\mathbf{B}_b\big], \quad (70)$$

where the $\widetilde{\text{SMSE}}$ indicates the upper bound of SMSE in (66). We also define $\varphi_f \triangleq 2\alpha_{\mathbf{\Delta H}_f}\sigma_{\max}(\hat{\mathbf{H}}_f)+\alpha^2_{\mathbf{\Delta H}_f}$ and $\varphi_H \triangleq 2\alpha_{\mathbf{\Delta H}}\sigma_{\max}(\hat{\mathbf{H}}^H)+\alpha^2_{\mathbf{\Delta H}}$. Indeed, the upper bound of SMSE in (70) is a direct consequence of the following bounds:

$$\hat{\mathbf{H}}_f\mathbf{\Delta H}_f^H+\mathbf{\Delta H}_f\hat{\mathbf{H}}_f^H+\mathbf{\Delta H}_f\mathbf{\Delta H}_f^H \le 2\alpha_{\mathbf{\Delta H}_f}\sigma_{\max}(\hat{\mathbf{H}}_f)+\alpha^2_{\mathbf{\Delta H}_f}\mathbf{I}_K \quad (71)$$

$$\hat{\mathbf{H}}^H\mathbf{\Delta H}+\mathbf{\Delta H}^H\hat{\mathbf{H}}+\mathbf{\Delta H}^H\mathbf{\Delta H} \le 2\alpha_{\mathbf{\Delta H}}\sigma_{\max}(\hat{\mathbf{H}}^H)+\alpha^2_{\mathbf{\Delta H}}\mathbf{I}_N \quad (72)$$

$$\mathbf{\Delta H}_f\mathbf{\Delta HB}+\mathbf{B}^H\mathbf{\Delta H}_f^H\mathbf{\Delta} \ge -2\frac{\alpha_{\mathbf{\Delta H}}\alpha_{\mathbf{\Delta H}_f}}{\sigma_{\min}(\mathbf{B}^H\mathbf{B})}\sigma_{max}(\mathbf{B})\mathbf{B}^H\mathbf{B} \quad (73)$$

$$\mathbf{\Delta H}_f\hat{\mathbf{H}}\mathbf{B}+\mathbf{B}^H\mathbf{\Delta H}_f^H\hat{\mathbf{H}}^H \ge -2\frac{\alpha_{\mathbf{\Delta H}_f}\sigma_{\max}(\hat{\mathbf{H}})}{\sigma_{\min}(\mathbf{B}^H\mathbf{B})}\sigma_{max}(\mathbf{B})\mathbf{B}^H\mathbf{B} \quad (74)$$

$$\hat{\mathbf{H}}_f\mathbf{\Delta HB}+\mathbf{B}^H\hat{\mathbf{H}}_f^H\mathbf{\Delta H}^H \ge -2\frac{\alpha_{\mathbf{\Delta H}}\sigma_{\max}(\hat{\mathbf{H}}_f)}{\sigma_{\min}(\mathbf{B}^H\mathbf{B})}\sigma_{max}(\mathbf{B})\mathbf{B}^H\mathbf{B}, \quad (75)$$

where we assume $\sigma_{\max}(\mathbf{B})=1$, $\sigma_{\min}(\mathbf{B}^H\mathbf{B})=1$ and optimizing these parameters are left for future works. Eventually, the optimal designs of $\mathbf{B}_a$ and $\mathbf{B}_b$ can be obtained as

$$\frac{\partial \widetilde{\text{SMSE}}}{\partial \mathbf{B}_a} = 0 \rightarrow \mathbf{B}_a = \hat{\mathbf{H}}^H(\hat{\mathbf{H}}^H\hat{\mathbf{H}}+\varphi_H\mathbf{I}_N)^{-1} \quad (76)$$

$$\frac{\partial \widetilde{\text{SMSE}}}{\partial \mathbf{B}_b} = 0 \rightarrow \mathbf{B}_b = (\hat{\mathbf{H}}_f\hat{\mathbf{H}}_f^H+\varphi_f\mathbf{I}_K)^{-1}\hat{\mathbf{H}}_f^H, \quad (77)$$

which are optimized the $\widetilde{\text{SMSE}}$ in (70) to

$$\widetilde{\text{SMSE}} = \text{trace}\big[\frac{1}{\kappa_B}\mathbf{I}_K-(\hat{\mathbf{H}}^H\hat{\mathbf{H}}+\varphi_H\mathbf{I}_N)^{-1}\big(\hat{\mathbf{H}}\hat{\mathbf{H}}^H\hat{\mathbf{H}}_f\hat{\mathbf{H}}_f^H+2 (\alpha_{\mathbf{\Delta H}}\alpha_{\mathbf{\Delta H}_f}-\alpha_{\mathbf{\Delta H}_f}\sigma_{\max}(\hat{\mathbf{H}})-\alpha_{\mathbf{\Delta H}}\sigma_{\max}(\hat{\mathbf{H}}_f))\big)(\hat{\mathbf{H}}_f\hat{\mathbf{H}}_f^H+\varphi_f\mathbf{I}_K)^{-1}\big]. \quad (78)$$

Notably, the proposed $\mathbf{B}_a$ in (76) and $\mathbf{B}_b$ in (77) are ZF schemes that include regularized factors of φ_H and φ_f, respectively.

VI. Numerical Results

In order to further compare the performance of the proposed scenarios in this study, Monte Carlo simulations have been carried out. The simulation setup is based on an array fed reflector antenna/feed provided by European Space Agency (ESA) in the context of SatNexIII project with $N = 154$ feeds and $K = 100$ beams, at each time instant, which serve a single user per beam spread over the whole Europe [17].

Results have been averaged for a total of 500 channel realizations. The detail of simulation parameters are collected in

TABLE I
UL SIMULATION PARAMETERS

Parameter	Value
Satellite height	35786 km (geostationary)
Satellite longitude, latitude	$10°East, 0°$
Frequency	20×10^9
Earth radius	6378.137 Km
Feed radiation pattern	Provided by ESA [17]
Number of feeds N	154
Number of beams	100
Carrier frequency	20 GHz (Ka band)
Total bandwidth	500 MHz
Atmospheric fading	Just rain fading [17]
Roll-off factor	0.25
User antenna gain	41.7 dBi
clear sky gain	17.68 dB/K

Table I. Note that the channel fading statistics corresponds to the city of Rome.

As a performance metric, we compute the SINR for each user, after interference mitigation and then its throughput (bit/s) is inferred according to DVB-S2x standard for a packet error rate (PER) of 10^{-6} [23].

For a best practice and in order to clarify the performance of proposed BMGP architectures, we consider the following reference scenarios:

1) Upper-bound reference, a single GW multibeam architecture, i.e. $F = 1$, is conceived where a linear ZF precoding is embedded at the GW aiming to mitigate inter-beam interference as well as the satellite works in transparent mode $\mathbf{B} = (\mathbf{I})_{N\times K}$ (see GP architecture in Section I.B.1). In this context, the mathematical expression of the ZF precoding scheme can be written as

$$\mathbf{T} = \mathbf{H}_{ref}^H(\mathbf{H}_{ref}\mathbf{H}_{ref}^H)^{-1}, \quad (79)$$

where $\mathbf{H}_{ref} \triangleq \mathbf{H}$ in case of analyzing the P-BMGP network and $\mathbf{H}_{ref} \triangleq \mathbf{H}\mathbf{H}_f$ for both SGN-BMGP and SN-BMGP networks. It is evident that the precoding in (79) can mitigate the interference in the UL for P-BMGP architecture and it is capable to reject the interference in both UL and FL of SGN-BMGP and SN-BMGP architectures. Even if the dimension employed in MGP leads to drastically increase in the available FL bandwidth resource, however, this dimension limits the effectiveness of the interference mitigation techniques and therefore the system throughput is decreased with respect to the single GW scenario [6]-[9].

2) Lower-bound reference, developing the BFN in BMGP network through the Discrete Fourier Transform (DFT) approach which is detailed in [24]. For the ground segment, the precoding in (33) is used.

A. P-BMGP architecture

This section presents the simulation results related to the scenarios described in Section III. A total of $F = 14$ GWs is considered so that each GW serves a cluster of 7 or 8 beams, i.e. $K_m = 7$ or 8. The number of employed feeds per GW is $N_m = 11$. Note that the analysis in Section III assumes an identical number of beams per cluster; in practice, this can be easily extended to heterogeneous configurations as the one provided by ESA [17]. Remarkably, the effect of inter-FL interference is neglected for the P-BMGP architecture. The allocated power to all clusters is the same, e.g. $P_m = \frac{P}{F}$.
The nature of the employed fed reflector antenna imposes the fact that $N_m < K_{-m}$ degree of freedom is available and the performance analysis of the proposed signal processing schemes in Sections III should be adapted with this constraint. For the proposed P-BMGP architecture, the following schemes are compared:
(i) The upper bound reference.
(ii) ESA benchmark in P-BMGP (ESA-PBMGP): the precoding in (33) and the BFN provided by ESA in the context of SatNex III project [17].
(iii) Adaptive Processing in P-BMGP (AP-PBMGP): the precoding in (33) and the channel adaptive design of $\mathbf{B}$ in (40).
(iv) Fixed Processing in P-BMGP (FP-PBMGP): the precoding in (33) and the non-channel adaptive design of $\mathbf{B}$ in (49).
(v) The lower bound reference.

Figure. 2 (left) depicts the evolution of the total average

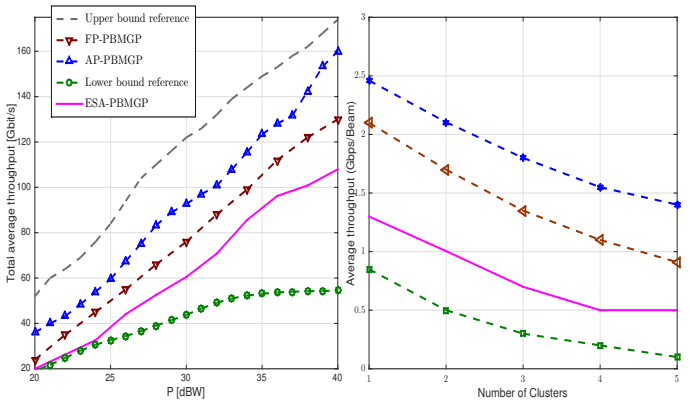

Fig. 2. Average total throughput (Gbits/s) comparison in P-MGWP network based on DVB-S2x MODCOD (Left). Average throughput per beam versus number of clusters (Right).

throughput (Gbits/s) as a function of P. As it is expected, the AP-PBMGP provides a significant gain with respect to the upper bound reference scenario. This is due to its capability to adaptively cope with the inter- and intra-cluster interference at each GW. Since each GW employs the ZF precoding design in (33), the performance of proposed $\mathbf{B}$ characterized by Equation (49), i.e. FP-PBMGP, is also illustrated in Figure 2 (left). This scheme shows small performance improvement versus the lower bound reference, and the ESA-PBMGP one, and furthermore, it provides an acceptable results with respect to the AP-PBMGP. This is due to the robustness of the proposed FP-PBMGP while the UL channel varies by time.
Figure 2 (right) also compares the results of the proposed schemes in (i)-(v) considering that each GW receives interference from 1 to 5 clusters. The transmit power is set to $P = 35dBW$. Evidently, even with only one interfering cluster, the average throughput decreases. Indeed, the larger the number of clusters, the more significant the effect of inter- and intra cluster interference is. Nevertheless, a performance improvement comes from the presented AP- and FP-PBGMP with respect to the other scenarios.
The improvement can be also noticed from the corresponding robustness plots in Fig. 3. In this context, we study the impact

TABLE II
β_H, β_V AND β_f MEASUREMENT FOR A TOTAL OF F CLUSTERS.

Feed selec. Mech.	$m = 1, .., 14$ (11 feed/cluster)
β_H	$10^{-2} \sim 10^{-3}$
β_V	$10^{-1} \sim 10^{-2}$
β_f	$10^{-1} \sim 10^{-3}$

of the UL channel variations on the FP-PBGMP. Bearing in mind that the operators ϵ_H and ϵ_V in (104) determine the UL channel variation. It is worth to note that, the values of ϵ_V and ϵ_H are selected so that the feasibility of $\breve{\mathbf{S}}_m$ in Theorem 1 holds. It implies that

$$(\lambda_{max}(\hat{\mathbf{H}}_m\hat{\mathbf{H}}_m^H) - \epsilon_H)^+ > 0, \quad (80)$$

$$(\lambda_{max}(\hat{\mathbf{V}}_{-m}^0\hat{\mathbf{V}}_{-m}^{0,H}) - \epsilon_V)^+ > 0. \quad (81)$$

For a large value of ϵ_H or/and ϵ_V the expression (80) or/and (81) might become negative which changes the nature of the problem. In order to avoid this, the ϵ_H and ϵ_V have to be checked so that the right terms in (80) and (81) always remain positive. To overcome such excessive pessimism, it is necessary to include in ϵ_H and ϵ_v respectively the additional factors β_H and β_V which should be found by numerical simulations. In such a condition, the expressions in (80) and (81) shall be rewritten by $(\lambda_{max}(\hat{\mathbf{H}}_m\hat{\mathbf{H}}_m^H) - \beta_H\epsilon_H)^+ > 0$ and $(\lambda_{max}(\hat{\mathbf{V}}_{-m}^0\hat{\mathbf{V}}_{-m}^{0,H}) - \beta_V\epsilon_V)^+ > 0$. The order of β_H and β_V obtained by numerical simulations are collected in Table II.

B. SGN-BMGP and SN-BMGP architectures

The subsection deals with the numerical results of SGN-BMGP and SN-BMGP architectures in Sections IV and V. For the sake of illustration, we assume the following simple inter-FL interference model for matrix $\mathbf{H}_f$ [9]:

$$\mathbf{H}_{f,m} = \mathbf{I}_{K_m}, \quad (82)$$

$$\mathbf{H}_{f,mi} = \rho_{mi}^{|m-i|}\mathbf{E}_{K_m} \quad m \neq i, \quad (83)$$

for $m = 1, ..., F$ and $i = 1, ..., F$. The matrix $\mathbf{H}_{f,mi}$ denotes the interference power level received by the m-th GW from the i-th GW with $m \neq i$. The expression (82) implies that each GW transmits signals to the satellite through a free intra-FL interference communication link. The parameter $\rho_{mi} \in [0, 1]$ is a parameter that models the overall interference gain level between the m-th and the i-th GW FLs. We consider $\rho_{mi} = 1$, which is a worst-case scenario.
The following scenarios compare in this subsection:
(i) The lower bound reference scenario.
(ii) The upper bound reference scenario.
(iii) ESA benchmark in SGN-BMGP (ESA-SGNBMGP): the precoding in (33) and the on-board processing $\mathbf{B}$ provided by ESA in [17].
(iv) Adaptive Processing in SGN-BMGP (AP-SGNBMGP): the precoding in (53) and the channel adaptive design of $\mathbf{B}$ in Section IV-A.
(v) Fixed Processing in SGN-BMGP (FP-SGNBMGP): the

precoding in (55) and the non-channel adaptive design of $\mathbf{B}$ in (64).
(vi) Adaptive joint Processing in SN-BMGP (AP-SNBMGP): the channel adaptive on-board processings in (67) and (68).
(vii) Fixed joint Processing in SN-BMGP (FP-SNBMGP): the fixed on-board processings in (76) and (77).
(viii) The FP-PBMGP scheme in Section VI.A.
Figure 4 (Left) depicts the total average throughput of the proposed scenarios in the SGN-BMGP and the SN-BMGP networks versus the different power levels. It is evident the dramatical effect of inter-FL interference reduces the performance of the SGN-BMGP and SN-BMGP architectures with respect to the P-BMGP even though precoding and BFN are performed. It can be observed that the AP-SNBMGP offers a throughput similar to the upper bound reference. Indeed, this AP-SNBMGP scheme is able to properly mitigate the interference in both UL and FL. In addition, the AP-SGNBMGP provides a slightly close outcome with respect to the upper bound reference scenario. However, the effectiveness of the AP-SGNBMGP is reduced due to the fact that the

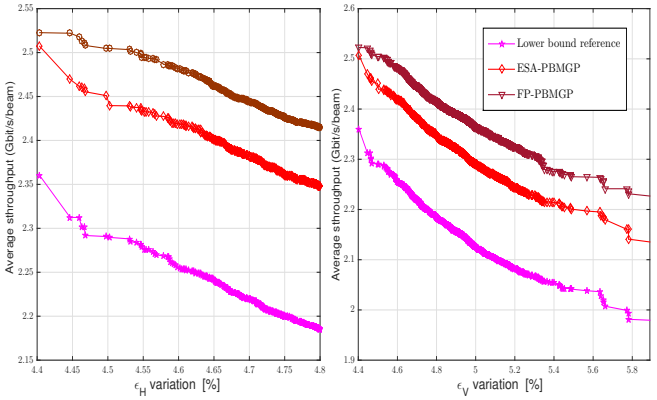

Fig. 3. Throughput with respect to the UL channel variations ϵ_H (Left) and ϵ_V (Right).

dimension of the SGN-BMGP architectures intuitively limits the performance of the precoding scheme, and therefore the throughput is decreased in front of the upper bound scenario. The results in Fig. 4 (Left) also show that both FP-PBMGP and FP-SGNBMGP have close performance. This implies that the precoding scheme in (53) can reject the inter-FL interference in the SGN-BMGP networks, however, the proposed FP-PBMGP architecture outperforms the presented FP-SGNBMGP. As a matter of fact, the robustness of the proposed FP-PBMGP with respect to the UL channel variation is tighter than the same scheme in the FP-SGNBMGP. Moreover, the configurations in both SGN-BMGP and SN-BMGP present better performance than the ESA- SGNBMGP and the lower bound reference.
Figure 4 (Middle) justifies the expected result of throughputs in Fig. 4 (Left) considering that each GW receives interference from 1 to 5 GWs. The transmit power is set to $P = 28dBW$. Evidently, even with only one interfering GW, the average throughput decreases with respect to the ideal FL scenario in P-BMGP. Interestingly, our proposed FP-SGNBMGP and FP-SNBMGP provide acceptable performance versus the rest of scenarios. Figure 4 (Right) shows the performance of our proposals in SGN-BMGP and SN-BMGP for different values of ρ. It is observed that a large amount of variation ρ in the FLs leads to a degradation of the system performance. Nevertheless, our proposed schemes provide a potential advantage in order to compensate throughput degradation through the impact of inter-FL, intra- and inter- cluster interference.
The robustness plots in Fig. 5 are also noticed the improvement of the throughput gain matching the robustness performance. We study the impact of the UL and FL channel variations in the context of FP-SGNBMGP and FP-SNBMGP architectures. Note that the notations ϵ_H and ϵ_f in (104) determine the UL and FL channels variations in SGN-BMGP

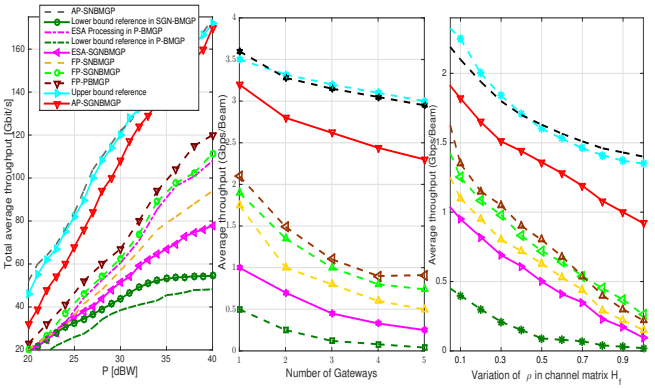

Fig. 4. Average total throughput (Gbits/s) comparison in P-MGWP network based on DVB-S2x MODCOD (Left). The number of GWs/clusters is 14. Average throughput per beam versus number of clusters (Middle). Average throughput per beam for different amounts of inter-FL interference ρ in the channel matrix $\mathbf{H}_f$ (Right).

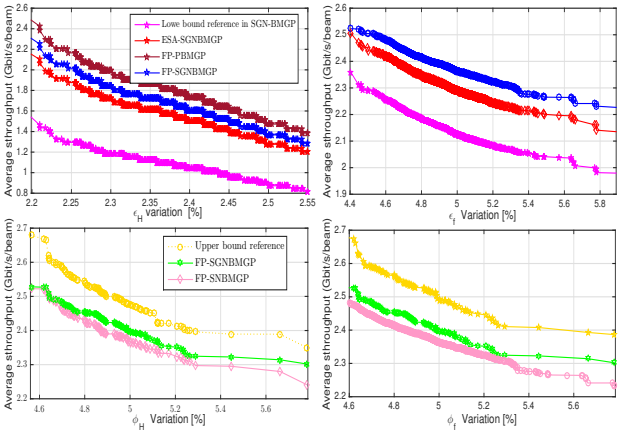

Fig. 5. Throughput with respect to channel variations ϵ_H (Top-Left), ϵ_f (Top-Right), φ_H (Bottom-Left) and φ_f (Bottom-Right).

network. The parameters φ_H and φ_f denote the impact of the user and FL channels variations in SN-BMGP network as well. These values are computed and their corresponding average throughput are presented in Figure 5. Note that, analogous to the presented bounds for ϵ_H and ϵ_V respectively in (80) and (81), the values of ϵ_f shall be selected so that the feasibility of $\breve{\mathbf{M}}_m$ in Theorem 2 holds. It implies that the sufficient condition is to have: $(\sum_{i\neq m} \frac{\kappa_{f,m}}{\kappa_{f,i}} (\lambda_{max}(\hat{\mathbf{H}}_{mi}\hat{\mathbf{H}}_{mi}^H) - \epsilon_f)^+) > 0$. To this end, an additional factor β_f is necessary to use, i.e. $(\sum_{i\neq m} \frac{\kappa_{f,m}}{\kappa_{f,i}} (\lambda_{max}(\hat{\mathbf{H}}_{mi}\hat{\mathbf{H}}_{mi}^H) - \beta_f\epsilon_f)^+)$, which quantize through numerical simulations. The order of β_f is projected in Table II.

VII. Conclusion

This paper dealt with designing joint precoding and BFN of a MGP architecture. The analyzed MGP architecture suffers from i) a large intra-cluster, inter-cluster and inter-FL interference; and ii) high cost due to providing a fair balance between available FL resources and data demand growth.

Under an analytic framework, we showed that implementing a proper on-board BFN (e.g. preferably non-channel adaptive) at the MGP architecture leads to considerable diminish in the required FL resources while imposing only a low computation complexity is targeted. Moreover, we developed several ZF precoding techniques adapted with the proposed on-broad BFN in order to cope with the increased level of inter-cluster, intra-cluster and inter-FL interference. We applied the proposed precoding schemes in the following premises: (a) each GW construct a part of the full ZF precoding matrix, b) the satellite and GWs perform the precoding scheme, and (c) a joint design of ZF precoding and on-board BFN is implemented at the payload.

Appendix A

The goal here is to prove that

$$\begin{aligned}&\text{trace}\left(\mathbf{B}_m^H\mathbf{Q}_m^H(\mathbf{Q}_m\mathbf{Q}_m^H)^{-2}\mathbf{Q}_m\mathbf{B}_m\right)\\&\geq \text{trace}\left(\mathbf{B}_m^{\star,H}\mathbf{Q}_m^H(\mathbf{Q}_m\mathbf{Q}_m^H)^{-2}\mathbf{Q}_m\mathbf{B}_m^{\star}\right).\end{aligned}\tag{84}$$

By employing decomposition of the $\mathbf{Q}_m$ in (29), for the right hand side of inequality (84) we can have that

$$\text{trace}\left(\mathbf{B}_m^{\star,H}\mathbf{Q}_m^H(\mathbf{Q}_m\mathbf{Q}_m^H)^{-2}\mathbf{Q}_m\mathbf{B}_m^{\star}\right)=\sum_i\lambda_i\left(\mathbf{M}_m\right)\tag{85}$$

with

$$\mathbf{M}_m\triangleq\mathbf{V}_{-m}^{0,H}\mathbf{H}_m^H(\mathbf{H}_m\mathbf{V}_{-m}^0\mathbf{V}_{-m}^{0,H}\mathbf{H}_m^H)^{-2}\mathbf{H}_m\mathbf{V}_{-m}^0,\tag{86}$$

where $\lambda_i(.)$ denotes the i-th eigen value of the respective matrix.

On the other hand, the left hand side of inequality (84) can be written as

$$\begin{aligned}\text{trace}\left(\mathbf{B}_m^H\mathbf{Q}_m^H(\mathbf{Q}_m\mathbf{Q}_m^H)^{-2}\mathbf{Q}_m\mathbf{B}_m\right)&=\sum_i\lambda_i\left(\mathbf{B}_m^H\mathbf{V}_{-m}^0\mathbf{M}_m\mathbf{V}_{-m}^{0,H}\mathbf{B}_m\right)\\&=\sum_i\lambda_i\left(\mathbf{V}_{-m}^{0,H}\mathbf{B}_m\mathbf{B}_m^H\mathbf{V}_{-m}^0\mathbf{M}_m\right).\end{aligned}\tag{87}$$

Applying Lemma H.1.g in [25] to (87) holds

$$\begin{aligned}&\sum_i\lambda_i\left(\mathbf{V}_{-m}^{0,H}\mathbf{B}_m\mathbf{B}_m^H\mathbf{V}_{-m}^0\mathbf{M}_m\right)\\&\geq\sum_i\lambda_{K_m-i+1}\left(\mathbf{V}_{-m}^{0,H}\mathbf{B}_m\mathbf{B}_m^H\mathbf{V}_{-m}^0\right)\lambda_i\left(\mathbf{M}_m\right).\end{aligned}\tag{88}$$

Since $(\mathbf{V}_{-m}^{0,H}\mathbf{B}_m\mathbf{B}_m^H\mathbf{V}_{-m}^0)$ is a semidefinite positive matrix (with $\lambda_{(K_m-i+1)}\left(\mathbf{V}_{-m}^{0,H}\mathbf{B}_m\mathbf{B}_m^H\mathbf{V}_{-m}^0\right)\geq 0$), we have that

$$\sum_i\lambda_{(K_m-i+1)}\left(\mathbf{V}_{-m}^{0,H}\mathbf{B}_m\mathbf{B}_m^H\mathbf{V}_{-m}^0\right)\lambda_i\left(\mathbf{M}_m\right)\geq\sum_i\lambda_i\left(\mathbf{M}_m\right).\tag{89}$$

Appendix B

The objective here is to prove the Theorem 1.

First, from (29) and (45) we have

$$\mathbf{Q}_m\mathbf{Q}_m^H=\mathbf{H}_m\mathbf{V}_{-m}^0\mathbf{V}_{-m}^{0,H}\mathbf{H}_m^H=\mathbf{H}_m(\mathbf{R}_{V,-m}+\mathbf{R}_{\Delta V,-m})\mathbf{H}_m^H,\tag{90}$$

where

$$\mathbf{R}_{V,-m}\triangleq\hat{\mathbf{V}}_{-m}^0\hat{\mathbf{V}}_{-m}^{0,H},\tag{91}$$

$$\mathbf{R}_{\Delta V,-m}\triangleq\hat{\mathbf{V}}_{-m}^0\boldsymbol{\Delta}\mathbf{V}_{-m}^{0,H}+\boldsymbol{\Delta}\mathbf{V}_{-m}^0\hat{\mathbf{V}}_{-m}^0+\boldsymbol{\Delta}\mathbf{V}_{-m}^0\boldsymbol{\Delta}\mathbf{V}_{-m}^{0,H}.\tag{92}$$

With employing the upper bound of the uncertainity region $||\boldsymbol{\Delta}\mathbf{V}_{-m}^0||\leq\alpha_{\boldsymbol{\Delta}\mathbf{V}_{-m}^0}$ in (47), we can apply Lemma 7.1 in [22] to bound $(\mathbf{R}_{V,-m}+\mathbf{R}_{\Delta V,-m})$ as follows:

$$\hat{\mathbf{V}}_{-m}^0\hat{\mathbf{V}}_{-m}^{0,H}\leq\lambda_{max}(\hat{\mathbf{V}}_{-m}^0\hat{\mathbf{V}}_{-m}^{0,H})\mathbf{I}_{N_m},\tag{93}$$

$$\begin{aligned}&\boldsymbol{\Delta}\mathbf{V}_{-m}^0\hat{\mathbf{V}}_{-m}^0+\boldsymbol{\Delta}\mathbf{V}_{-m}^0\boldsymbol{\Delta}\mathbf{V}_{-m}^{0,H}\\&\leq 2\sigma_{max}(\hat{\mathbf{V}}_{-m}^0)\sigma_{max}(\boldsymbol{\Delta}\mathbf{V}_{-m}^0)\mathbf{I}_{N_m}\leq 2\sigma_{max}(\hat{\mathbf{V}}_{-m}^0)\alpha_{\boldsymbol{\Delta}\mathbf{V}_{-m}^0}\mathbf{I}_{N_m},\end{aligned}\tag{94}$$

$$\begin{aligned}&\boldsymbol{\Delta}\mathbf{V}_{-m}^0\boldsymbol{\Delta}\mathbf{V}_{-m}^{0,H}\\&\leq\lambda_{max}(\boldsymbol{\Delta}\mathbf{V}_{-m}^0\boldsymbol{\Delta}\mathbf{V}_{-m}^{0,H})\mathbf{I}_{N_m}\leq\sigma_{max}^2(\boldsymbol{\Delta}\mathbf{V}_{-m}^0)\mathbf{I}_{N_m}\leq\alpha_{\boldsymbol{\Delta}\mathbf{V}_{-m}^0}^2\mathbf{I}_{N_m}.\end{aligned}\tag{95}$$

where $\lambda_{\max}(.)$ and $\sigma_{\max}(.)$ represent the maximum eigenvalue and singular value of the corresponding matrix, respectively.

Applying the upper bounds in (93)-(95), the SVD of $\mathbf{R}_{V,-m}=\mathbf{U}_{V,-m}\boldsymbol{\Sigma}_{V,-m}\mathbf{U}_{V,-m}^H$ establishes the upper- and lower- bounds of $(\mathbf{R}_{V,-m}+\mathbf{R}_{\Delta V,-m})$ as follows

$$\begin{aligned}&\mathbf{U}_{V,-m}\big(\boldsymbol{\Sigma}_{V,-m}+\epsilon_V\mathbf{I}_{N_m}\big)\mathbf{U}_{V,-m}^H\\&\geq(\mathbf{R}_{V,-m}+\mathbf{R}_{\Delta V,-m})\geq(\lambda_{max}(\hat{\mathbf{V}}_{-m}^0\hat{\mathbf{V}}_{-m}^{0,H})-\epsilon_V)^+\mathbf{I}_{N_m}\end{aligned}\tag{96}$$

where $\epsilon_V\triangleq(2\alpha_{\boldsymbol{\Delta}\mathbf{V}_{-m}^0}\sigma_{\max}(\hat{\mathbf{V}}_{-m}^0)+\alpha_{\boldsymbol{\Delta}\mathbf{V}_{-m}^0}^2)$.

With (44), the term $\mathbf{H}_m\mathbf{H}_m^H$ in (90) can be decomposed as

$$\mathbf{H}_m\mathbf{H}_m^H=\mathbf{R}_{H,m}+\mathbf{R}_{\Delta,m},\tag{97}$$

where

$$\mathbf{R}_{H,m}\triangleq\hat{\mathbf{H}}_m\hat{\mathbf{H}}_m^H,\tag{98}$$

$$\mathbf{R}_{\Delta,m}\triangleq\hat{\mathbf{H}}_m\boldsymbol{\Delta}\mathbf{H}_m^H+\boldsymbol{\Delta}\mathbf{H}_m\hat{\mathbf{H}}_m^H+\boldsymbol{\Delta}\mathbf{H}_m\boldsymbol{\Delta}\mathbf{H}_m^H.\tag{99}$$

Following steps similar to the those for the derivation of equation (96), using $||\boldsymbol{\Delta}\mathbf{H}_m||\leq\alpha_{\boldsymbol{\Delta}\mathbf{H}_m}$, and the SVD of $\mathbf{R}_{H,m}=\mathbf{U}_{H,m}\boldsymbol{\Sigma}_{H,m}\mathbf{U}_{H,m}^H$, we can obtain

$$\begin{aligned}&\mathbf{U}_{H,m}(\boldsymbol{\Sigma}_{H,m}+\epsilon_H\mathbf{I}_{K_m})\mathbf{U}_{H,m}^H\\&\geq\big(\mathbf{R}_{H,m}+\mathbf{R}_{\Delta,m}\big)\geq(\lambda_{max}(\hat{\mathbf{H}}_m\hat{\mathbf{H}}_m^H)-\epsilon_H)^+\mathbf{I}_{K_m}\end{aligned}\tag{100}$$

where $\epsilon_H\triangleq 2\alpha_{\boldsymbol{\Delta}\mathbf{H}_m}\sigma_{\max}(\hat{\mathbf{H}}_m^H)+\alpha_{\boldsymbol{\Delta}\mathbf{H}_m}^2$.

Note that some values of ϵ_V and ϵ_H in (100) lead to $(\lambda_{max}(\hat{\mathbf{V}}_{-m}^0\hat{\mathbf{V}}_{-m}^{0,H})-\epsilon_V)<0$ and $(\lambda_{max}(\hat{\mathbf{H}}_m\hat{\mathbf{H}}_m^H)-\epsilon_H)<0$, respectively. To avoid this issue, the value of ϵ_V and ϵ_H have to be checked and, if necessary, decreased such that the $(\lambda_{max}(\hat{\mathbf{V}}_{-m}^0\hat{\mathbf{V}}_{-m}^{0,H})-\epsilon_V)^+$ and $(\lambda_{max}(\hat{\mathbf{H}}_m\hat{\mathbf{H}}_m^H)-\epsilon_H)^+$ remain positive.

Given (96) and (100), the following lower bound is fulfilled

$$\mathbf{Q}_m\mathbf{Q}_m^H\geq(\lambda_{max}(\hat{\mathbf{H}}_m\hat{\mathbf{H}}_m^H)-\epsilon_H)^+(\lambda_{max}(\hat{\mathbf{V}}_{-m}^0\hat{\mathbf{V}}_{-m}^{0,H})-\epsilon_V)^+\mathbf{I}_{K_m},\tag{101}$$

which corresponds to

$$(\mathbf{Q}_m\mathbf{Q}_m^H)^{-2}\leq\big((\lambda_{max}(\hat{\mathbf{H}}_m\hat{\mathbf{H}}_m^H)-\epsilon_H)^+(\lambda_{max}(\hat{\mathbf{V}}_{-m}^0\hat{\mathbf{V}}_{-m}^{0,H})-\epsilon_V)^+\big)^{-2}\mathbf{I}_{K_m}.\tag{102}$$

In addition, similar to (101) the upper bound of $\mathbf{Q}_m^H\mathbf{Q}_m$ can be obtained by

$$\begin{aligned}&\mathbf{Q}_m^H\mathbf{Q}_m=\mathbf{V}_{-m}^0\mathbf{V}_{-m}^{0,H}\mathbf{H}_m^H\mathbf{H}_m\mathbf{V}_{-m}^0\mathbf{V}_{-m}^{0,H}\\&=(\mathbf{R}_{V,-m}+\mathbf{R}_{\Delta V,-m})\big(\mathbf{R}_{H,m}+\mathbf{R}_{\Delta,m}\big)^H(\mathbf{R}_{V,-m}+\mathbf{R}_{\Delta V,-m})\\&\leq\mathbf{U}_{V,-m}(\boldsymbol{\Sigma}_{V,-m}+\epsilon_V\mathbf{I}_{N_m})\mathbf{U}_{V,-m}^H\mathbf{U}_{H,m}(\boldsymbol{\Sigma}_{H,m}^H+\epsilon_H\mathbf{I}_{N_m})\mathbf{U}_{H,m}^H\\&\qquad\mathbf{U}_{V,-m}\big(\boldsymbol{\Sigma}_{V,-m}+\epsilon_V\mathbf{I}_{N_m}\big)\mathbf{U}_{V,-m}^H\end{aligned}\tag{103}$$

If the bounds in (102) and (103) are valid, for (48) we have

$$\begin{aligned}&\mathbf{Q}_m^H(\mathbf{Q}_m\mathbf{Q}_m^H)^{-2}\mathbf{Q}_m\\&\leq\breve{\mathbf{S}}_m\triangleq\big((\lambda_{max}(\hat{\mathbf{H}}_m\hat{\mathbf{H}}_m^H)-\epsilon_H)^+(\lambda_{max}(\hat{\mathbf{V}}_{-m}^0\hat{\mathbf{V}}_{-m}^{0,H})-\epsilon_V)^+\big)^{-2}\\&\qquad\mathbf{U}_{V,-m}\big(\boldsymbol{\Sigma}_{V,-m}+\epsilon_V\mathbf{I}_{N_m}\big)\mathbf{U}_{V,-m}^H\mathbf{U}_{H,m}(\boldsymbol{\Sigma}_{H,m}^H+\epsilon_H\mathbf{I}_{N_m})\mathbf{U}_{H,m}^H\\&\qquad\mathbf{U}_{V,-m}\big(\boldsymbol{\Sigma}_{V,-m}+\epsilon_V\mathbf{I}_{N_m}\big)\mathbf{U}_{V,-m}^H.\end{aligned}\tag{104}$$

Then, applying the inequality in (104) implies the upper bound of (48) as

$$\text{trace}\left(\mathbf{B}_m^H\mathbf{Q}_m^H(\mathbf{Q}_m\mathbf{Q}_m^H)^{-2}\mathbf{Q}_m\mathbf{B}_m\right)\leq\text{trace}\left(\mathbf{B}_m^H\breve{\mathbf{S}}_m\mathbf{B}_m\right).\tag{105}$$

Finally, by using the SVD of $\breve{\mathbf{S}}_m=\breve{\mathbf{L}}_m\breve{\boldsymbol{\Omega}}_m\breve{\mathbf{L}}_m^H$, the set of BFN submatrices $\mathbf{B}_m$ in (48) are obtained as

$$\mathbf{B}_m^{\star}=\breve{\mathbf{L}}_m\begin{pmatrix}\mathbf{U}_{H,m}\\\mathbf{w}\end{pmatrix}\qquad,m=1,\ldots,F\tag{106}$$

where $\mathbf{w}$ of size $(N_m-K_m)\times K_m$ is a zero matrix. Indeed, $\mathbf{B}_m$ in (106) guarantees

$$\text{trace}\left(\mathbf{B}_m^H\breve{\mathbf{S}}_m\mathbf{B}_m\right)\geq\text{trace}\left(\mathbf{B}_m^{\star,H}\breve{\mathbf{S}}_m\mathbf{B}_m^{\star}\right).\tag{107}$$

The sketch of the proof of (107) is similar to Appendix A.

APPENDIX C

The goal here is to prove the Theorem 2.

Similar to the bounds in (95), the following lower bound is realized for the problem (63):

$$\begin{aligned}\mathbf{B}_m^H(\sum_{i\neq m}\frac{\kappa_m}{\kappa_i}\mathbf{H}_{mi}^H\mathbf{H}_{mi})\mathbf{B}_m \\ = \mathbf{B}_m^H\Big(\sum_{i\neq m}\frac{\kappa_m}{\kappa_i}(\hat{\mathbf{H}}_{mi}+\boldsymbol{\Delta}\mathbf{H}_{mi})^H(\hat{\mathbf{H}}_{mi}+\boldsymbol{\Delta}\mathbf{H}_{mi})\Big)\mathbf{B}_m \\ \geq \sum_{i\neq m}\frac{\kappa_m}{\kappa_i}\big(\lambda_{max}(\hat{\mathbf{H}}_{mi}\hat{\mathbf{H}}_{mi}^H)-\epsilon_f\big)^+\mathbf{I}_{K_m}, \qquad (108)\end{aligned}$$

where $\epsilon_f \triangleq 2\alpha_{\boldsymbol{\Delta}\mathbf{H}_{mi}}\sigma_{\max}(\hat{\mathbf{H}}_{mi}^H)+\alpha_{\boldsymbol{\Delta}\mathbf{H}_{mi}}^2$.

Given (100) and (108), the following upper bounds hold

$$\begin{aligned}\Big(\mathbf{B}_m^H\mathbf{H}_m^H\mathbf{H}_m\mathbf{B}_m+\mathbf{B}_m^H(\sum_{i\neq m}\frac{\kappa_m}{\kappa_i}\mathbf{H}_{mi}^H\mathbf{H}_{mi})\mathbf{B}_m\Big)^{-1} \\ \leq\Big(\big(\sum_{i\neq m}\frac{\kappa_m}{\kappa_i}\lambda_{max}(\hat{\mathbf{H}}_{mi}\hat{\mathbf{H}}_{mi}^H)-\epsilon_f\big)^+ +\big(\lambda_{max}(\hat{\mathbf{H}}_m\hat{\mathbf{H}}_m^H)-\epsilon_H\big)^+\Big)^{-1}\mathbf{I}_{K_m}, \qquad (109)\end{aligned}$$

and

$$\begin{aligned}\text{trace}\Big\{\Big(\mathbf{B}_m^H\mathbf{H}_m^H\mathbf{H}_m\mathbf{B}_m+\mathbf{B}_m^H(\sum_{i\neq m}\frac{\kappa_m}{\kappa_i}\mathbf{H}_{mi}^H\mathbf{H}_{mi})\mathbf{B}_m\Big)^{-1} \\ \mathbf{B}_m^H\mathbf{H}_m^H\mathbf{H}_m\mathbf{B}_m\Big\} \leq \mathbf{B}_m^H\breve{\mathbf{M}}_m\mathbf{B}_m, \qquad (110)\end{aligned}$$

with

$$\begin{aligned}\breve{\mathbf{M}}_m \triangleq \Big(\big(\sum_{i\neq m}\frac{\kappa_{f,m}}{\kappa_{f,i}}\lambda_{max}(\hat{\mathbf{H}}_{mi}\hat{\mathbf{H}}_{mi}^H)-\epsilon_f\big)^+\big) \\ +(\lambda_{max}(\hat{\mathbf{H}}_m\hat{\mathbf{H}}_m^H)-\epsilon_H)^+\Big)^{-1}\mathbf{U}_{H,m}(\boldsymbol{\Sigma}_{H,m}+\epsilon_H\mathbf{I}_{K_m})\mathbf{U}_{H,m}. \qquad (111)\end{aligned}$$

Eventually, with the SVD of $\breve{\mathbf{M}}_m = \breve{\mathbf{S}}_m\breve{\boldsymbol{\Psi}}_m\breve{\mathbf{S}}_m^H$, the optimal design of $\mathbf{B}_m$ is obtained as

$$\mathbf{B}_m^\star = \breve{\mathbf{S}}_m\begin{pmatrix}\mathbf{U}_{H,m}\\ \mathbf{w}\end{pmatrix} \qquad ,m=1,\ldots,F \qquad (112)$$

which establishes

$$\text{trace}\left(\mathbf{B}_m^H\breve{\mathbf{M}}_m\mathbf{B}_m\right) \geq \text{trace}\left(\mathbf{B}_m^{\star,H}\breve{\mathbf{M}}_m\mathbf{B}_m^\star\right), \qquad (113)$$

where $\mathbf{w}$ is expressed in (106). The sketch of the proof in (113) is similar to Appendix A and left due to space brevity.

REFERENCES

[1] Daniel Minoli, "Innovations in satellite communications technology," in *John Wiley & Sons Inc. Hoboken, USA, 2015.*

[2] J.D. Gayrard, "Terabit satellite: Myth or reality?" in *First International Conference on Advances in Satellite and Space Communications (SPACOMM), pp. 1-6 , July 2009.*

[3] G. Zheng, S. Chatzinotas and B. Ottersten, "Generic optimization of linear precoding in multibeam satellite systems, in *IEEE Transactions on Wireless Communications, vol. 11, no. 6, pp. 2308-2320, 2012.*

[4] L. Cottatellucci, M. Debbah, E. Casini, R. Rinaldo, R. Mueller, M. Neri and G. Gallinaro, "Interference mitigation techniques for broadband satellite system," in *24th AIAA International Satellite Communications Systems Conference, June 2006, USA.*.

[5] A. Gharanjik, B. Rao. Shankar, P. D. Arapoglou and B. Ottersten, "Gateway switching in Q/V band satellite feeder links," in *IEEE Letter of Communications, vol. 17, no. 7, pp. 1384-1387, July 2013.*

[6] J. Arnau, B. Devillers, C. Mosquera and A. Perez-Neira, "Performance study of multiuser interference mitigation schemes for hybrid broadband multibeam satellite architectures, " in *EURASIP Journal on Wireless Communications and Networking, 2012.*

[7] J. Tronc, P. Angeletti, N. Song, M. Haardt, J. Arendt, and G. Gallinaro, "Overview and comparison of on-ground and on-board beamforming techniques in mobile satellite service applications," in *International Journal of Satellite Communications and Networking, no. 4291-308, 2013.*

[8] G. Zheng, S. Chatzinotas and B. Ottersten, "Multi-gateway cooperation in multibeam satellite systems," in *23rd IEEE International Symposium on Personal, Indoor and Mobile Radio Communications, 2012, USA.*

[9] V. Joroughi, M. A. Vzquez and A. I. Prez-Neira, "Precoding in multigateway multibeam satellite systems," in *IEEE Transactions on Wireless Communications, Vol. 15, No. 7, pp. 1-13, July 2016.*

[10] V. Boussemart, M. Berioli, F. Rossetto, and M. Joham, "On the achievable rates for the return-link of multibeam satellite systems using successive interference cancellation," in *Military Communications Conference (MILCOM), pp. 217-223, Nov 2011.*

[11] B. Devillers, A. Perez-Neira and C. Mosquera, "Joint linear precoding and beamforming for the forward link of multi-beam broadband satellite systems," in *IEEE Global Telecommunications Conference (GLOBECOM), pp. 1-6, December 2011, USA.*

[12] V. Joroughi, M. A. Vazquez, A. Ana Perez-Neira and B. Devillers, "Design of an on board beam generation process for a multibeam broadband satellite system," in *IEEE Transactions on Wireless Communications, Vol. 13, pp. 1-14, March 2017.*

[13] V. Joroughi, M. A. Vazquez, and A. Perez-Neira, "Multiple gateway precoding with per feed power constraints for multibeam satellite systems," in *Proceedings of 20th European Wireless Conference , pp. 1-7, May 2014, Spain.*

[14] SM Kay,"Fundamentals of statistical signal processing: estimation theory," in *Prentice-Hall Inc. Upper Saddle River, 1993, USA.*

[15] B. Devillers and A. Perez-Neira, "Advanced interference mitigation techniques for the forward link of multi-beam broadband satellite systems," in *Conference Record of the Forty Fifth Asilomar Conference on Signals, Systems and Computers, pp. 1810-1814, November 2011, USA.*

[16] Y. Silva and A. Klein, "Linear transmit beamforming techniques for the multigroup multicast scenario," in *IEEE Transactions on Vehicular Technology, vol. 58, no. 8, pp. 4353-4367, October 2009.*

[17] Call of Order 2-Task 1, "Fair comparison and combination of advanced interference mitigation techniques," Satellite Network of Experts (SatNEx) 3, report of ESAcontract NO:23089/10/NL/CPL.

[18] D. Palomar, J. Cioffi and M. A. Lagunas, "Joint Tx-Rx beamforming design for multicarrier MIMO channels: a unified framework for convex optimization," in *IEEE Transactions on Signal Processing, vol. 51, no. 9, pp. 2381-2401, September 2003.*

[19] J. Wang and D. Palomar, "Worst-case robust mimo transmission with imperfect channel knowledge," in *IEEE Transactions on Signal Processing, vol. 57, no. 8, pp. 3086-3100, August 2009.*

[20] A. Pascual-Iserte, D. Palomar, A. Perez-Neira and M. Lagunas, "A robust maximin approach for MIMO communications with imperfect channel state information based on convex optimization, in *IEEE Transactions on Signal Processing, vol. 54, no. 1, pp. 346-360, January 2006.*

[21] G. H. Golub and C. F. Van Loan, "Matrix computations (3rd Ed.)" *Johns Hopkins University Press, 1996, USA.*

[22] D. P. Palomar, "A unified framework for communications through MIMO channels," in *Ph.D. dissertation, Technical University of Catalonia (UPC), May 2003, Spain.*

[23] ETSI EN 302 307-2: "Digital Video Broadcasting (DVB); Second generation framing structure, channel coding and modulation systems for Broadcasting, Interactive Services, News Gathering and other broadband satellite applications; Part 2: DVB-S2 Extensions (DVB-S2X)."

[24] I. Thibault, B. Devillers, E. Candreva, F. Lombardo, A. Vanelli-Coralli, and G. Corazza, "Joint feeder-link bandwidth compaction and interference mitigation based on a hybrid space/ground processing architecture for a broadband multibeam satellite system," in *International Journal of Satellite Communications and Networking, vol. 32, no. 2, pp. 107-125, 2014.* [Online]. Available: http://dx.doi.org/10.1002/sat.1042.

[25] AW. Marshall and I. Olkin, "Inequalities: theory of majorization and its applications," in *Academic Press, 1979, USA.*